UNIVERSITY *of York*

This is a repository copy of *Modeling lightning-NOx chemistry at sub-grid scale in a global chemical transport model*.

White Rose Research Online URL for this paper:
https://eprints.whiterose.ac.uk/92560/

Version: Published Version

Article:

White Rose
university consortium
Universities of Leeds, Sheffield & York

eprints@whiterose.ac.uk
https://eprints.whiterose.ac.uk/

Atmospheric
Chemistry
and Physics
Discussions

Open Access

Modeling lightning-NO$_x$ chemistry at sub-grid scale in a global chemical transport model

A. Gressent[1], B. Sauvage[1], D. Cariolle[2,3], M. Evans[4,5], M. Leriche[1], C. Mari[1], and V. Thouret[1]

[1]LA, CNRS, Université Paul Sabatier III de Toulouse, Toulouse, France
[2]Météo France, Toulouse, France
[3]Centre Européen de Recherche et de Formation Avancée en Calcul Scientifique, CERFACS, Toulouse, France
[4]Wolfson Atmospheric Chemistry Laboratories (WACL), Department of Chemistry, University of York, York, YO10 5DD, UK
[5]National Centre for Atmospheric Science (NCAS), University of York, York, YO10 5DD, UK

Correspondence to: A. Gressent (alicia.gressent@aero.obs-mip.fr)

ACPD

15, 34091–34147, 2015

Modeling lightning-NO$_x$ chemistry at sub-grid scale

A. Gressent et al.

Title Page

Abstract | Introduction

Conclusions | References

Tables | Figures

◀ | ▶

◀ | ▶

Back | Close

Full Screen / Esc

Printer-friendly Version

Interactive Discussion

Abstract

For the first time, a plume-in-grid approach is implemented in a chemical transport model (CTM) to parameterize the effects of the non-linear reactions occurring within high concentrated NO$_x$ plumes from lightning NO$_x$ emissions (LNO$_x$) in the upper tro-

5 posphere. It is characterized by a set of parameters including the plume lifetime, the effective reaction rate constant related to NO$_x$-O$_3$ chemical interactions and the fractions of NO$_x$ conversion into HNO$_3$ within the plume. Parameter estimates were made using the DSMACC chemical box model, simple plume dispersion simulations and the mesoscale 3-D Meso-NH model. In order to assess the impact of the LNO$_x$ plume ap-

10 proach on the NO$_x$ and O$_3$ distributions at large scale, simulations for the year 2006 were performed using the GEOS-Chem global model with a horizontal resolution of 2° × 2.5°. The implementation of the LNO$_x$ parameterization implies NO$_x$ and O$_3$ decrease at large scale over the region characterized by a strong lightning activity (up to 25 and 8 %, respectively, over Central Africa in July) and a relative increase downwind

15 of LNO$_x$ emissions (up to 18 and 2 % for NO$_x$ and O$_3$, respectively, in July) are derived. The calculated variability of NO$_x$ and O$_3$ mixing ratios around the mean value according to the known uncertainties on the parameter estimates is maximum over continental tropical regions with ΔNO$_x$ [−33.1; +29.7] ppt and ΔO$_3$ [−1.56; +2.16] ppb, in January, and ΔNO$_x$ [−14.3; +21] ppt and ΔO$_3$ [−1.18; +1.93] ppb, in July, mainly depending on

20 the determination of the diffusion properties of the atmosphere and the initial NO mixing ratio injected by lightning. This approach allows (i) to reproduce a more realistic lightning NO$_x$ chemistry leading to better NO$_x$ and O$_3$ distributions at the large scale and (ii) focus on other improvements to reduce remaining uncertainties from processes related to NO$_x$ chemistry in CTM.

1 Introduction

Lightning emissions are one of the most important sources of nitrogen oxides (NO$_x$ ≡ NO + NO$_2$) in the upper troposphere (WMO, 1999; Hudman et al., 2007). Lightning emitted NO$_x$ (LNO$_x$) impact the tropospheric ozone burden (Stockwell et al., 1999;

5 Hauglustaine et al., 2001; Grewe, 2007), and the hydroxyl-radical (OH) concentrations influencing the oxidizing capacity of the atmosphere (Labrador et al., 2004; Banerjee et al., 2014). Lightning flashes including cloud-to-ground and intra-cloud flashes produce reactive nitrogen species which are detrained in the cloud anvil (Weiss et al., 2012) and released directly in the upper troposphere. Because of an ozone production

10 efficiency (OPE) 4 to 20 times larger in the upper troposphere than in the middle or low troposphere (Sauvage et al., 2007a; Martin et al., 2007), effects of LNO$_x$ on chemistry are expected to be stronger in the upper troposphere (Pickering et al., 1990; Hauglustaine et al., 1994; Zhang et al., 2003; Choi et al., 2009). The longer NO$_x$ lifetime in the upper troposphere (1–2 weeks) allows the long-range transport of LNO$_x$ through the

15 large circulation patterns (Hemispheric Transport of Air Pollution, HTAP report, 2010: http://www.htap.org/).

Although the importance of the LNO$_x$ emissions on the upper tropospheric chemistry is well known, it remains highly uncertain with a best estimate of 2–8 Tg N yr^{-1} (Schumann and Huntrieser, 2007). Lightning NO$_x$ emissions are associated with deep

20 convection (horizontal scale ∼ 10 km) and correspond to the "sub-grid" in global chemical transport models (horizontal resolution hundreds of kilometers). This implies that the impact of the lightning NO$_x$ emissions should be parameterized for inclusion into a large scale model. Global models commonly used convection proxies such as the cloud-top-height (Price and Rind, 1992) and the updraft intensity to estimate the light-

25 ning flashes. Flashes simulated by CTMs are commonly constrained by satellite observations (Sauvage et al., 2007b; Murray et al., 2012) such as measurements from the space-borne Lightning Imaging Sensor (LIS) and the Optical Transient Detector (OTD) on TRMM (Christian et al., 2003; Tost et al., 2007). The lightning NO$_x$ emissions are

A. Gressent et al.

then redistributed according to a vertical profile generally a "C-Shape" profile (Pickering et al., 1998) a priori defined depending on season, latitude and continent/ocean location. Also, corrections on the calculations of lightning NO$_x$ emissions using satellite observations (SCIAMACHY, Martin et al., 2007) and in-situ measurements (INTEX-NA, Hudman et al., 2007) are usually applied.

Despite the success in simulating the lightning NO$_x$ emissions, the small scale nature of the flashes and the non-linear chemistry (Lin et al., 1988) of the atmosphere will lead to biases on the large scale with instantaneous dilution of gases in the large grid box volume. It seems likely that this will lead to an overestimate of the OPE and an underestimate of the nitric acid (HNO$_3$) production. For instance, by forcing NO$_x$ concentration in GEOS-Chem grid box over Southeast Asia to represent the measured lightning plumes, Cooper et al. (2014) estimate a ratio for O$_3$ to HNO$_3$ produced leading to a 15 mol mol^{-1} OPE in lightning plumes, that reinforces the fact that instantaneous dilution in global model implies issues in sub-grid chemistry.

In this work, a realistic lightning NO$_x$ chemistry as well as a plume parameterization is implemented into a global chemical transport model (CTM) allowing reproducing more accurately the large scale NO$_x$ and O$_3$ distributions. The plume approach used in this study was previously developed by Cariole et al. (2009) for aircraft NO$_x$ emissions in the LMDz-INCA and MOBIDIC models and also implemented to deal with the ship NO$_x$ emissions (Huszar et al., 2010). This approach avoids the double count in the CTM calculation of the emitted NO$_x$, first instantaneously diluted into the point grid and second as the plume form. In addition, the plume parameterization is the first that considers the NO$_x$ from lightning as a plume with the transport of the related non-linear chemistry effects. NO$_x$ from lightning emissions are emitted in the upper troposphere characterized by strong winds that allows large scale transport of trace species. Thus, it is relevant to consider a plume growth from lightning emissions, which could be diluted long time after the initial lightning pulse, downwind of emissions. Consequently, the plume parameterization previously developed for aircraft exhausts has been adjusted

to LNO$_x$ emissions and implemented into the GEOS-Chem global chemical transport model.

Section 2 gives a description of the GEOS-Chem model in which the plume-in-grid parameterization is implemented and models used to evaluate the diffusion properties of the atmosphere and to determine parameters characterizing the physics and chemistry of the lightning NO$_x$ plume. A concise description of the plume approach is then presented in Sect. 3 followed by a detailed explanation of the determination of parameters related to LNO$_x$ emissions. Section 4 summarizes the results of the simulations performed with GEOS-Chem and finally these results and the sensitivity on NO$_x$ and O$_3$ variations of the parameterization are discussed in Sect. 5.

2 Models

Three different models are used in this evaluation and are described in this section. GEOS-Chem is used to provide a global framework to assess the impact of lightning NO$_x$. Meso-NH is used to provide estimates of the plume diffusion timescales and DSMACC is a box model used to assess the non-linear chemistry in the plume.

2.1 The GEOS-Chem chemical transport model

The GEOS-Chem chemical transport model (Bey et al., 2001) is a global 3-D model of atmospheric composition driven by assimilated meteorology from the Goddard Earth Observing System (GEOS-5) of the NASA Global Modeling Assimilation Office (GMAO). The 09-01-01 version (http://wiki.seas.harvard.edu/geos-chem/index.php/GEOS-Chem_v9-01-01) of the CTM has been used in this study. The model transports 43 tracers to describe tropospheric O$_3$-NO$_x$-VOC chemistry. The horizontal resolution is 2° × 2.5° and 47 vertical levels are defined from the ground to 80 km altitude. The CTM includes modules for emissions, transport, chemistry, deposition, aerosols and surface.

The large-scale advection of tracers is performed using the TPCORE advection scheme (Lin and Rood, 1996) corresponding to a semi-lagrangian flux method. Shallow and deep moist convection processes are carried out using the Relaxed Arakawa–Schubert scheme (Moorthi and Suarez, 1991). Mixing in the lower atmospheric layers is represented by a non-local scheme of the planetary boundary layer described by Lin and McElroy (2010). The wet deposition for water-soluble aerosols and for gases follows Liu et al. (2001) and Amos et al. (2012). Aerosol scavenging by ice crystals and cold/mixed precipitation is also reproduced in the model (Wang et al., 2011). The dry deposition is associated to a scheme which calculates bulk surface resistance in series (Wesely, 1989). Photolysis rates are calculated with the Fast-JX code (Bian and Prather, 2002). The atmospheric chemistry is resolved using the SMVGEAR solver (Jacobson and Turco, 1994) with more than 300 species and 785 chemical reactions. Heterogeneous chemical reactions are represented on the surface of the sulfate aerosols (Bey et al., 2001) and mineral dust (Martin et al., 2002). Effects of aerosols on the photolysis rates are based on Martin et al. (2003). Primary NO_x and VOCs (Volatile Organic Compounds) emissions are separated depending on sources. Global anthropogenic emissions are given by the GEIA (Wang et al., 1998) and EGDAR (Olivier, 2005) inventories and regional anthropogenic emissions are specially estimate for US (NEI05), Canada (CAC), Mexico (BRAVO), Europe (EMEP) and East Asia (Streets et al., 2006; Zhang et al., 2009). Fossil fuel emissions are provided by EPA and STREETS 2006 inventories (Yevich and Logan, 2003), biomass burning emissions by GFED inventory (Lobert et al., 1999), and biogenic emissions by the MEGAN model calculations (Guenther et al., 2012). In addition, NO_x from soil emissions are calculated by an algorithm depending on temperature and precipitation (Yienger and Levy, 1995).

The lightning NO_x emissions calculation is initially based on the cloud-top-height parameterization (Price and Rind, 1992, 1994) with a "C-shaped" profile describing LNO_x vertical distribution (Pickering et al., 1998; Ott et al., 2010). Lightning flashes are constrained using the climatologies from the LIS/OTD observations (Sauvage et al.,

2007b; Murray et al., 2012). Global lightning NO$_x$ emissions are also constrained to 6 Tg N yr^{-1} in order to match to satellite observations (Martin et al., 2007).

2.2 The Meso-NH model

The Meso-NH model is an atmospheric model developed jointly by the Laboratoire d'Aérologie and by CNRM-GAME (http://mesonh.aero.obs-mip.fr/mesonh51). The model includes a non-hydrostatic and anelastic system of equations (Lafore et al., 1998) and has a complete set of parameterizations allowing to reproduce physical processes such as radiation (Gregory et al., 2000), atmospheric turbulence (Cuxart et al., 1999), convection (Bechtold et al., 2000), microphysics related to warm clouds (Cohard and Pinty, 2000), and atmospheric ice (Pinty and Jabouille, 1999; Lascaux et al., 2006). Meso-NH includes also on-line chemistry (Tulet et al., 2003, 2006). The model deals with large (synoptic) to small (large eddy) scales. In this study, the Mesonh-49 version was used in order to compare the horizontal diffusion coefficient (D_h) estimate within the anvil of thunderstorms from in-situ measurements to a modeling ideal case of a convective cell.

2.3 The DSMACC chemical box model

The Dynamical Simple Model of Atmospheric Chemical Complexity (DSMACC) is a simple box model developed for improving our understanding of the tropospheric chemistry (Emmerson and Evans, 2009). The model is composed of the KPP chemical pre-processor (Damian et al., 2002) to solve differential equations representing the chemical system. The TUV (Tropospheric Ultraviolet and Visible Radiation Model) photolysis scheme is used, which calculates the spectral irradiance, the spectral actinic flux, photodissociation coefficients (J values) (Madronich and Flocke, 1999), and biologically effective irradiance. The chemical scheme used derives from the Master Chemical Mechanism (MCM, http://mcm.leeds.ac.uk/MCM/), (Jenkin et al., 1997;

Saunders et al., 2003), which contains 17 000 elementary reactions of 6700 primary, secondary and radical species.

In order to study the chemical interactions that could occur in the undiluted plume fraction, a set of short simulations was carried out with the DSMACC chemical box model as explained in the Sect. 3.2.2.

3   Plume parameterization for lightning NO$_x$ emissions

3.1   General description

The LNO$_x$ plume parameterization is based on a method initially developed by Cariolle et al. (2009) for NO$_x$ emissions related to aircraft exhausts later adapted to ship emissions of NO$_x$ (Huszar et al., 2010). In this approach, the plume effects at sub-grid scale are represented via a fuel tracer, to follow the amount of the emitted species in the plume and an effective reaction rate for the ozone production and nitric acid production/destruction during the plume's dilution into the background (Cariolle et al., 2009; Paoli et al., 2011). The parameterization requires a proper estimation of the characteristic plume lifetime during which the non-linear interactions between species are important and simulated via specific rates of conversion. The approach ensures the mass conservation of species in the model. This is the only method which considers a plume evolution related to the local NO$_x$ emissions allowing the transport of the non-linear effects occurring at smaller scale than the model grid.

3.1.1   Physical plume formulation

Following Cariolle et al. (2009), a passive tracer (from the perspective of the usual model chemistry) is added to the model to represent NO$_x$ emitted by lightning. Rather than increasing the concentration of the NO$_x$ tracer in the model, lightning NO$_x$ emissions now increase the concentration of this new tracer which is transported in the

standard way by advection and turbulence. Plume chemistry is considered to be significant when the concentration of the lightning NO_x tracer is higher than a critical NO_x content, hereafter denoted r_l. Above this value the lightning NO_x tracer is transferred to the normal NO_x tracer at a rate described by a plume lifetime (τ), which is an exponential decay constant. This corresponds to an exchange time scale between the lightning NO_x plume and the background NO_x. The continuity equation related to the tracer evolution is detailed by the Eq. (1).

$$\frac{\partial \overline{r_{LNO_x}}}{\partial t} + \langle F_{LNO_x} \rangle = I - \frac{1}{\tau} \times \overline{r_{LNO_x}} \tag{1}$$

where $\overline{r_{LNO_x}}$, is the concentration (in molecules cm^{-3}) of the NO_x lightning tracer in the model grid (note that all overlined terms referred to grid average quantities in the CTM), $F_{LNO_x} \equiv \nabla \times (\overline{r_{LNO_x}} u) + \nabla \times (D_t \nabla \overline{r_{LNO_x}})$ and it corresponds to the flux divergence related to the large-scale transport of the tracer (advection and turbulent diffusion, in molecules cm^{-3} s^{-1}), I is the injection rate of NO_x (in molecules cm^{-3} s^{-1}) and τ is the plume lifetime (in seconds).

The calculation of τ requires evaluating the mass fraction of the lightning NO_x ($M(t)$) corresponding to the undiluted fraction of the plume and characterized by a NO_x concentration above the r_l critical value. In other words, the plume boundary is defined by the critical value r_l depending on the time of day. The NO_x mass, $M(t)$ decreases monotonically to zero until $t = T_l$ for which the tracer concentration is everywhere below the r_l threshold. The plume lifetime is obtained by an exponential function depending on the mass (Eqs. 2 and 3):

$$M(t) = \int_{V_p} \rho \times r_p \times dV \tag{2}$$

$$\tau = \int_{t_0=0}^{+\infty} \exp(-t/\tau) \times dt = \frac{1}{M(t_0)} \int_{t_0=0}^{T_l} M(t) \times dt \tag{3}$$

Title Page

Abstract | Introduction

Conclusions | References

Tables | Figures

|◄ | ►|

◄ | ►

Back | Close

Full Screen / Esc

Printer-friendly Version

Interactive Discussion

where V_p is the volume of the plume, ρ is the density of the air, r_p is the NO$_x$ concentration within the plume (molecules cm^{-3}) and T_l is the time for which the concentration r_p is everywhere below the critical value r_l. The calculation of the plume lifetime, by simple plume dispersion simulations, depends on (i) the initial emissions of NO$_x$ by lightning,

5 (ii) the r_l value, and (iii) the dispersion properties of the atmosphere (related to the horizontal diffusion coefficient, D_h) and is detailed on the Sect. 3.2.3. Note that the mean dispersion properties of the atmosphere were associated with the horizontal diffusion only. The vertical diffusion is less efficient than the horizontal one (Cariolle et al., 2009) and it is not considered in this study. In addition, the vertical dispersion of the plume is

10 related to the vertical distribution of LNO$_x$ a priori forced in the GEOS-Chem model by the C-shape profile (Ott et al., 2010) and it is beyond the scope of this study.

3.1.2 Plume chemistry of NO$_x$, O$_3$ and HNO$_3$

Once the lightning NO$_x$ is emitted, it is transferred to model's background NO$_x$ based on the lifetime of the plume (τ). Thus, the continuity equation for the NO$_x$ species

15 emitted in the plume and released to the large scale can be deduced as described by the Eq. (4).

$$\frac{\partial \overline{r_{NO_x}}}{\partial t} + \langle F_{NO_x} \rangle = +\frac{1}{\tau} \times \overline{r_{LNO_x}} \times \alpha_{NO_x} \times EI_{NO_x} + L_{ss} \qquad (4)$$

where $\overline{r_{NO_x}}$, is the concentration of NO$_x$ (molecules cm^{-3}) in the model grid, α_{NO_x} is the molecular mass ratio between the air and NO$_x$ species, EI_{NO_x} is the emission index for

20 NO$_x$ (in g kg^{-1}) and L_{ss} are the large-scale sources and sinks (in molecules cm^{-3} s^{-1}) such as natural and anthropogenic emissions, photochemical reactions, mixing, and conversion to reservoir species.

We consider a fairly simple chemistry within the plume as described below. The increase of the nitrogen oxides concentration in the upper troposphere leads to ozone

25 production through the reaction of NO with peroxyde (HO$_2$), CH$_3$O$_2$, or RO$_2$ radicals

from the OH oxydation as shown by the Reaction (R1).

$$NO + RO_2 \longrightarrow NO_2 + RO \tag{R1}$$

In the case of large NO_x injection by lightning, the NO_x content (~ 40 ppt in unpolluted atmosphere) becomes of the same order (a few ppb, according to in-situ measurements, Dye et al., 2000; Huntrieser et al., 2002) than the surrounding ozone (60 ± 24 ppb) (Jaéglé et al., 1998). The ozone evolution within the plume is described by the Reactions (R2)–(R6).

$$NO_2 + h\nu(\lambda < 400\,nm) \longrightarrow NO + O \tag{R2}$$
$$NO + O_3 \longrightarrow NO_2 + O_2 \tag{R3}$$
$$O + O_2 + M \longrightarrow O_3 + M \tag{R4}$$
$$O + NO_2 \longrightarrow NO + O_2 \tag{R5}$$
$$O + O_3 \longrightarrow 2O_2 \tag{R6}$$
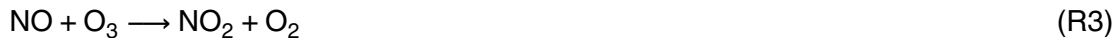
From these equations we can define an O_x family ($O_x \equiv O + O_2 + NO_2$) where the only net loss of O_x is by reactions between atomic oxygen and NO_2 or O_3. The sums of the concentrations as detailed by the Eqs. (5)–(7) (Cariolle et al., 2009).

$$\frac{d(O + O_3)}{dt} = +k_2 \times NO_2 - k_3 \times NO \times O_3 - k_5 \times O \times NO_2 - 2 \times k_6 \times O_3 \times O \tag{5}$$

$$\frac{d(O + O_3 + NO_2)}{dt} = -2 \times k_5 \times O \times NO_2 - 2 \times k_6 \times O_3 \times O \tag{6}$$

$$\frac{d(NO + NO_2)}{dt} = 0 \tag{7}$$

where k_i correspond to the rate constants for the R_i reactions.

Thus two processes occur to O_3 in the plume at daytime. On short timescales O_x is conserved. Lightning emissions of NO in the plume are converted into NO_2 but as NO_2 is in O_x family, there is net conservation of O_x. However, on long timescales O_x can be

destroyed through the reaction of O with NO_2 and O_3. Both of these processes need to be considered.

The first regime (regime I) occurs at low concentrations of NO_x (relative to O_3). Under these conditions the Reaction (R5) is slow. There is the rapid equilibrium between NO, NO_2 and O_3 (Reactions R2–R4). As a consequence, O_3 is converted into NO_2 and can be restored later after dilution of the plume depending on the balance between NO and NO_2 at the large scale (Cariolle et al., 2009). Overall O_x is conserved. In this regime NO emitted reacts with the available O_3 until the NO to NO_2 ratio in the plume reaches that in the background. Thus the impact on the O_3 background concentration is to reduce it by the number of molecules of NO emitted multiplied by the background NO_2 to NO_x ratio. The effect of the first regime on the ozone burden is expressed by the Eq. (8).

$$\frac{\partial \overline{r_{O_3}}}{\partial t} + \langle F_{O_3} \rangle = -\frac{1}{\tau} \times \overline{r_{LNO_x}} \times \alpha_{NO_x} \times EI_{NO_x} \times \left(\frac{\overline{NO_2}}{\overline{NO_x}} - E \right) \times \delta + L_{ss} \tag{8}$$

where $\overline{r_{O_3}}$ is the concentration of O_3 (molecules cm^{-3}) in the model grid, E is the $\frac{NO_2}{NO_x}$ ratio in the initial emissions, δ is equal to 1 during the day and 0 at nighttime, L_{ss} are the sources and sinks of ozone such as photochemical production, transport from the stratosphere, surface deposition, photolysis reactions, and photochemical destruction.

The second regime (regime II) occurs at high concentrations of NO_x (relative to O_3). Under these conditions the rate of Reaction (R5) is large. The non-linear chemical interactions between NO_x and O_3 occur with different rates than in the background atmosphere. To account for this, Cariolle et al. (2009) introduced an effective reaction rate constant (K_{eff}), which is related to the production or the destruction of the odd oxygen (O_x) within the plume. K_{eff} is expressed by the Eq. (9).

$$K_{eff} = \frac{\int_{t_0}^{T_l} \int_{V_p} K \times r_{NO_x}^{P} \times r_{O_3}^{P} \times dV_p \times dt}{\overline{r_{O_3}} \times \int_{t_0}^{t_l} \int_{V_p} r_{NO_x}^{P} \times dV_p \times dt} \tag{9}$$

where $r^{\mathrm{P}}_{\mathrm{NO}_x}$ and $r^{\mathrm{P}}_{\mathrm{O}_3}$ are the concentrations of nitrogen oxides and ozone within the plume and K is the rate of NO_x-O_3 reaction within the plume.

The analysis of the chemical reactions related to the two regimes shows that $\mathrm{O}_3 \gg \mathrm{O}$ and $k_5 \times \mathrm{NO}_2$ is more efficient than $k_6 \times \mathrm{O}_3$ as a sink for O_x (Cariolle et al., 2009). Thus, the Eq. (6) is simplified to give the Eq. (10).

$$\frac{\mathrm{d}(\mathrm{O}_3 + \mathrm{NO}_2)}{\mathrm{d}t} = -2 \times k_5 \times \mathrm{O} \times \mathrm{NO}_2 \tag{10}$$

Consequently, K_{eff} can be simplified to Eq. (11).

$$K_{\mathrm{eff}} = \frac{2 \times \left(\int^T k_5 \times \mathrm{O} \times \mathrm{NO}_2 \times \mathrm{d}t\right)}{\left(\mathrm{NO}_x \times \int^T \mathrm{O}_x \times \mathrm{d}t\right)} \tag{11}$$

The calculation of K_{eff} is detailed in Sect. 3.2.4. Considering the two regimes related to the sub-grid plume chemistry, the ozone burden is described by the Eq. (12) at daytime and nighttime. Note that at nighttime there is no direct impact due to the ozone plume chemistry on its burden as $\delta = 0$. Only indirect effects are expected from NO_y chemistry.

$$\frac{\partial \overline{r_{\mathrm{O}_3}}}{\partial t} + \langle F_{\mathrm{O}_3} \rangle = -\frac{1}{\tau} \times \overline{r_{\mathrm{LNO}_x}} \times \alpha_{\mathrm{NO}_x} \times \mathrm{EI}_{\mathrm{NO}_x} \times \left(\frac{\overline{\mathrm{NO}_2}}{\mathrm{NO}_x} - E\right) \times \delta - K_{\mathrm{eff}} \times \overline{r_{\mathrm{LNO}_x}} \times \rho$$

$$\times \alpha_{\mathrm{NO}_x} \times \mathrm{EI}_{\mathrm{NO}_x} \times \overline{r_{\mathrm{O}_3}} \times \delta + L_{\mathrm{ss}} \tag{12}$$

In addition, we consider the conversion of NO_x into HNO_3 within the plume. This conversion takes place in two different ways depending on the day or night atmospheric conditions. During the day, NO_2 reacts with OH to give HNO_3 directly and it is characterized by the coefficient β_1. While at nighttime the conversion of NO_x to HNO_3 occurs

through N_2O_5 formation followed by a heterogeneous hydrolysis reaction, which corresponds to β_2. These two fractions are unitless.

In summary, the equation system solved at large scale by the CTM for lightning NO_x source is detailed by the Eqs. (13)–(15).

$$\frac{\partial \overline{r_{NO_x}}}{\partial t} + \langle F_{NO_x} \rangle = +\frac{1}{\tau} \times \overline{r_{LNO_x}} \times (1 - \beta_1 \times \delta - \beta_2 \times (1 - \delta)) \times \alpha_{NO_x} \times EI_{NO_x} + L_{ss} \tag{13}$$

$$\frac{\partial \overline{r_{HNO_3}}}{\partial t} + \langle F_{HNO_3} \rangle = +\frac{1}{\tau} \times \overline{r_{LNO_x}} \times (\beta_1 \times \delta + \beta_2 \times (1 - \delta)) \times \alpha_{NO_x} \times EI_{NO_x} + L_{ss} \tag{14}$$

$$\frac{\partial \overline{r_{O_3}}}{\partial t} + \langle F_{O_3} \rangle = -\left(\frac{1}{\tau} \times \left(\frac{\overline{NO_2}}{\overline{NO_x}} - E\right) + K_{eff} \times \overline{r_{O_3}} \times \rho\right) \times \overline{r_{LNO_x}} \times \alpha_{NO_x}$$
$$\times EI_{NO_x} \times \delta + L_{ss} \tag{15}$$

where $\overline{r_{NO_x}}$, $\overline{r_{HNO_3}}$ and $\overline{r_{O_3}}$ correspond to the NO_x, HNO_3 and O_3 concentrations averaged over the grid cell of the model, respectively.

In this study, the tropospheric chemistry and especially the LNO_x plume chemistry is considered both at daytime and nighttime since all reactions are not initiated during the day. The chemical interactions during the night correspond mainly to the reactions of O_3 and O with NO and NO_2 as well as the NO_x deactivation and the chemistry of the nitrogen reservoir species (HNO_3, N_2O_5 and PAN) and the nitrate radical (NO_3). NO_3 is the main oxidant in night conditions and it is produced from the slow oxidation of NO_2 by O_3 (Reaction R7).

$$NO_2 + O_3 \longrightarrow NO_3 + O_2 \tag{R7}$$

The other dominant source of NO_3 is the destruction of N_2O_5 (Reaction R8), but as N_2O_5 is formed from NO_3 (Reaction R9), the two species act in a coupled manner.
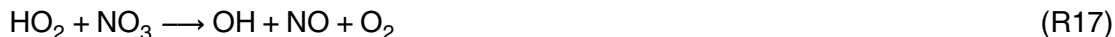
$$N_2O_5 + M \longrightarrow NO_3 + NO_2 + M \tag{R8}$$

$$\text{NO}_3 + \text{NO}_2 + \text{M} \longrightarrow \text{N}_2\text{O}_5 + \text{M} \tag{R9}$$

As mentioned previously, N_2O_5 is a determinant species for the tropospheric chemistry at nighttime allowing the HNO_3 formation by the heterogeneous reaction on the particle surface (aerosols and ice crystals). During the day, NO_3 rapidly undergo photolysis to produce NO or NO_2. In addition, NO_3 reacts very quickly with NO which is more concentrated at daytime than at nighttime (Reaction R10) but NO_3 is very low at daytime. However, this reaction can take place during the night especially for a plume characterized by high NO concentrations (lightning emissions) which is transported both during the day and night.

$$\text{NO}_3 + \text{NO} \longrightarrow \text{NO}_2 + \text{NO}_2 \tag{R10}$$

Furthermore, the nitrate radical can potentially reacts with VOCs. The reaction of the unsaturated hydrocarbons such as, isoprene, butenes, and monoterpenes, with NO_3 leads to the HNO_3 formation (Monks, 2005) (Reaction R11).

$$\text{NO}_3 + \text{RH} \longrightarrow \text{HNO}_3 + \text{R} \tag{R11}$$

Considering NO_3 reaction with alkenes, an additional mechanism is found initiating a complex chemistry allowing to form NO_2 or organic nitrates (Monks, 2005). Finally, NO_3 can initiate the VOCs oxidation via peroxy radical production (Reaction R12). That way, it can involve as a chain propagator (Reactions R13–R17).

$$\text{NO}_3 + \text{Organic Compound} \longrightarrow \text{R} + \text{Products} \tag{R12}$$
$$\text{R} + \text{O}_2 + \text{M} \longrightarrow \text{RO}_2 + \text{M} \tag{R13}$$
$$\text{RO}_2 + \text{NO}_3 \longrightarrow \text{RO} + \text{NO}_2 + \text{O}_2 \tag{R14}$$
$$\text{RO} + \text{O}_2 \longrightarrow \text{R}'\text{R}''\text{CO} + \text{HO}_2 \tag{R15}$$
$$\text{HO}_2 + \text{O}_3 \longrightarrow \text{OH} + 2\text{O}_2 \tag{R16}$$
$$\text{HO}_2 + \text{NO}_3 \longrightarrow \text{OH} + \text{NO} + \text{O}_2 \tag{R17}$$

The reactions of HO_2 with ozone (Reaction R16) or NO_3 (Reaction R17) imply OH production. Also, the reaction of ozone with alkenes allows to form OH during the night (Reaction R18) (Aumont, 2005).

$$Alkene + O_3 \longrightarrow v_1 OH + v_2 HO_2 + v_3 RO_2 \qquad (R18)$$

The Reaction (R18) occurs when ozone concentrations remain sufficiently high in night conditions, in other words for polluted atmosphere.

In this context, we consider different values at daytime and nighttime for the plume lifetime, the effective reaction rate constant and for the fraction of NO_x conversion into HNO_3 within the plume. Distinguishing day and night chemistry is linked with the fluctuation of the critical r_l value (below which the sub-grid plume chemistry is negligible) depending on atmospheric conditions. Therefore, if r_l changes with sunlight, the plume lifetime changes also. Note that except the β_2 fraction, this night chemistry is not considered by the initial plume approach developed by Cariolle et al. (2009), which considers NO_x plumes from aircraft exhausts only at daytime.

Figure 1 summarizes all elements which define the plume approach and how it has been adapted and implemented into the model.

3.2 Parameter calculations for lightning NO_x emissions

In order to reproduce more accurately the lightning NO_x sub-grid chemistry, some points should be considered: (i) the latitude (NO_x emissions by lightning are higher in tropics than in midlatitudes), (ii) the sunlight conditions (day and night) which impacts photochemistry and heterogeneous chemistry, (iii) the plume evolution with its own physical characteristics (the lifetime and the dispersion properties); and finally (iv) chemical interactions within the plume related to high concentrated fraction of NO_x considerably higher than background concentrations. In the following section, physical and chemical characteristics of the plume associated with lightning NO_x source have been defined.

3.2.1 Dynamical conditions

The horizontal diffusion coefficient (D_h) is a key parameter of the atmospheric dynamical conditions in determining the dispersion of the lightning NO$_x$ plume. D_h is used as the dispersion constraint for the simple plume dispersion simulations carried out in order to estimate the plume lifetime and the effective reaction rate constant. The diffusion coefficient was defined by running the 3-D mesoscale Meso-NH model but mainly from previous in-situ measurement in thunderstorm anvil.

The Meso-NH mesoscale model was used (see Sect. 2.2) to investigate D_h. A simple convective cell forced by warm bubble and initialized by a radiosounding at the beginning of the simulation was run as an ideal case. Simulations were realized for a domain of 24 km in the two horizontal directions and the grid horizontal resolution is $\Delta x = \Delta y = 1$ km and $\Delta z = 500$ m. The convective cell is located at 43.29° N latitude and 0° longitude (Klemp and Wilhelmson, 1978). Simulations of 6 h were made allowing the complete development and the dissipation of the convective cell. D_h has been calculated within the anvil using the mixing length diagnostic variable, hereafter denoted L, as described by the Eq. (16) (Cuxart et al., 1999).

$$D_h = \frac{2}{3} \times \frac{L}{4} \times e^{\frac{1}{2}} \tag{16}$$

At the mature stage of the cell, D_h was calculated as 100 m^2 s^{-1} within the upper levels of the convective cell (i.e. in the anvil, defined empirically).

In addition to modeling estimate, we used in-situ measurements to calculate D_h. Turbulence measurements were performed by a B-757 commercial aircraft along a fight from the west of Kansas to the north of Missouri and corresponding to a trajectory of more than 500 km (Trier and Sharman, 2008). These in-situ measurements were accomplished from 07:00 to 10:00 UTC the 17 June 2005, during the development of a mesoscale convective system (MCS). This MCS is associated with a turbulence event characterized by the measurement of the atmospheric eddy dissipation rate (ϵ) and the turbulence kinetic energy (TKE) above and within the cloud anvil. The higher values of ϵ

$(\epsilon^{1/3} \sim 0,4\,\mathrm{m^{2/3}\,s^{-1}})$ were recorded between 11.3 and 11.6 km altitude corresponding to the cloud anvil levels. In addition, for this MCS, the TKE was about $1\,\mathrm{m^2\,s^{-2}}$ at the locations of the highest ϵ values.

According to these observations, the turbulent diffusivity (Eq. 17) was estimated above the anvil of the MCS (http://www.ral.ucar.edu/projects/turb_char/) such as: $D_h > 0.1\,\mathrm{m^2\,s^{-2}}$. Then, D_h was calculated within the anvil such as: $D_h = 15\,\mathrm{m^2\,s^{-1}}$ using the same formulation (Eq. 17). This last estimate seems to be the most common value compared to the diffusion coefficient value of $20\,\mathrm{m^2\,s^{-1}}$ used by Cariolle et al. (2009), close to the tropopause level and the D_h value calculated for contrails ($15\,\mathrm{m^2\,s^{-1}}$) in the upper troposphere (Knollenberg, 1972).

$$D_h = \frac{(\mathrm{TKE})^2}{\epsilon} \tag{17}$$

The D_h estimate using Meso-NH model is high compared to the results from measurements and corresponds to the upper limit of the calculated diffusion coefficients and could be associated with the turbulence in the convective cloud. However, it is important to note that usually most numerical simulations are performed with 1-D turbulence models. What is interesting in the use of Meso-NH in this study is that the 3-D turbulence is solved. This simulation provides an additional estimate of D_h allowing comparison with the calculation from in-situ measurements. Moreover, studies on the diffusivity in cloud anvils are uncommon. It is necessary to conduct additional work in the future on that issue again constrained with new in-situ measurements of the atmospheric turbulence in the anvil.

In order to cover all of horizontal diffusivity estimates discussed in this section the range of values 0.1, 15 and $100\,\mathrm{m^2\,s^{-1}}$ was used. Hereafter, the results are detailed for the central value $D_h = 15\,\mathrm{m^2\,s^{-1}}$. Sensitivity tests depending on the uncertainty associated with the parameter estimate are performed and presented later in Sect. 4.3.

3.2.2 The NO$_x$ critical plume content (r_l)

The r_l critical value is the NO$_x$ concentration within the undiluted phase of the plume below which the non-linear chemistry can be neglected (Sect. 3.1). It has been estimated using the 0-D DSMACC chemical box model (Sect. 2.2). Initial conditions for simulations carried out with the DSMACC box model are from outputs of the GEOS-Chem model. Especially, initial atmospheric parameters and atmospheric background concentrations of species correspond to the average of the GEOS-Chem outputs (i) from 8 to 11 km, (ii) for two latitude regions (tropics and midlatitudes), and (iii) for the year 2006 (Table 1).

In order to focus on chemistry interactions only between chemical species of interest and removing the mixing influence and sunlight fluctuations, short simulations (i.e. one hour each) were run with the DSMACC model. The effects of the day or night conditions were carefully considered carrying out separate simulations at daytime and nighttime. Simulations were run for a large range of initial NO concentrations from 0.01 ppb to 1 ppm. The r_l value is defined from the NO value for which the $\frac{\partial O_x}{\mathrm{d}t}$ trend is perturbed. In other words, r_l is associated to the second derivative of O$_x$, i.e. the curve optimums on Fig. 2. The r_l threshold was defined as to be 0.1 and 0.25 ppb during the day and night for midlatitudes and 0.1 and 0.75 ppb during the day and night in tropics (Fig. 2).

Note that the midlatitudes and the tropics were separated because of the large differences in LNO$_x$ emissions between the two regions in terms of the number of flashes in a particular convective cell which is higher in the tropics according to the LIS/OTD climatologies (Christian et al., 2003). This last point is important for the plume lifetime estimate detailed in the following section.

3.2.3 The plume lifetime τ

The plume lifetime (τ) depends directly on (i) the initial NO pulse from lightning emissions, (ii) the r_l critical value, and (iii) the diffusion properties of the atmosphere. The plume lifetime also depends on the initial size of the plume. Here we use a width of

500 m to refer to an ensemble of spikes at the cloud scale. τ is crucial for the physical description of the NO_x plumes and it has been computed in carrying out dispersion simulations of a simple plume assumed to be cylindrical. The simple model is composed of 30 levels of dispersion. In the model, the standard atmospheric conditions are represented by temperature, pressure and species concentrations of the background atmosphere which are similar to the initial conditions used for the DSMACC simulations. As a reminder, initial conditions are from GEOS-Chem outputs averaged (i) from 8 to 11 km, (ii) for two latitude regions (tropics and midlatitudes), and (iii) for the year 2006 (Table 1). Simulations are initialized by a NO pulse from lightning emissions (hereafter denoted NO_i) and the plume dispersion depends on the D_h value estimated in Sect. 3.2.1.

The initial tracer concentrations NO_i related to lightning NO emissions at the scale of a convective cell (gathering several flashes together) in midlatitudes were defined according to previous aircraft measurement campaigns. Especially, the STERAO campaign recorded NO spikes of magnitude from 1–10 ppb related to lightning activity in thunderstorms occurring 9–10 July 1996 over the northern Colorado (Dye et al., 2000; Stith et al., 1999). Lange et al. (2001) measured NO spikes of 3.5 ppb during the STREAM campaign associated with a matured storm over the Ontario. Several peaks of NO mixing ratios from 0.7–6 ppb were also observed during EULINOX (Huntrieser et al., 2002) over Germany in July 1998. The LINOX aircraft campaign recorded NO spikes from 0.75–1.25 ppb (Huntrieser et al., 1998) related to thunderstorm over Europe, the 30 July 1996. From these studies, the NO concentration associated with the electrical activity in thunderstorms occurring over midlatitudes was determined as $NO_i^{mean, Midlats} = 3.4$ ppb ($NO_i^{min, Midlats} = 0.7$ and $NO_i^{max, Midlats} = 10$ ppb). Because there are much fewer LNO_x measurements in the tropics and in order to be consistent with the LNO_x emissions defined in the GEOS-Chem model, the ratio $R_{LNO_x} = \frac{LNO_x^{Midlatitudes}}{LNO_x^{Tropics}}$ was defined as in the CTM. During the year 2006, the relative midlatitudes and tropics LNO_x contribution was about $R_{LNO_x} = 0.33$. This result

Modeling lightning-NO_x chemistry at sub-grid scale

A. Gressent et al.

Title Page

Abstract	Introduction
Conclusions	References
Tables	Figures

|◀ | ▶|

| ◀ | ▶ |

| Back | Close |

Full Screen / Esc

Printer-friendly Version

Interactive Discussion

is in agreement with higher LNO$_x$ emissions in these regions rather than in midlatitudes. The value of NO mixing ratio injected by lightning in tropics was defined as NO$_i^{mean, Tropics}$ = 10.2 ppb (NO$_i^{min, Tropics}$ = 2.8 and NO$_i^{max, Tropics}$ = 29.7 ppb).

Once NO$_i$ estimate was completed, the calculation of the plume lifetime was achieved using the detailed formulation given in Sect. 3.1.1. The results for τ are summarized in Table 2. Hereafter, the results are detailed for NO$_i^{mean}$ in Sect. 4 and sensitivity tests are carried out using all NO$_i$ values for midlatitudes and tropics (Sect. 5). Model calculations for NO$_i^{mean}$ and D_h = 15 m^2 s^{-1} provide a minimum plume lifetime of 3 (6) h for midlatitudes and maximum plume lifetime of 9 (21.3) h for tropics at daytime (nighttime).

3.2.4 The effective reaction rate constant (K_{eff})

The non-linear chemistry within the plume has been considered in calculating the effective reaction rate constant (K_{eff}), which is used to compute the formation of the secondary species (O$_x$ and HNO$_3$) within the plume. That corresponds to the evolution of odd oxygen depending on the O and O$_3$ reactions with NO$_2$ and NO, and also on the NO$_x$ activation (day) or deactivation (night) with the HNO$_3$, N$_2$O$_5$ and PAN chemistry.

K_{eff} is calculated according to the Eq. (11) of the Sect. 3.1.2 using the same simple plume dispersion simulations than those carried out to define the plume lifetime (Sect. 3.2.3).

Results for K_{eff} are summarized in Table 3. Model calculations using NO$_i^{mean}$ and D_h = 15 m^2 s^{-1} give a K_{eff} value of 5.49 × 10^{-19} molecules^{-1} s^{-1} cm^{-3} (4.55 × 10^{-19} molecules^{-1} s^{-1} cm^{-3}) in midlatitudes and 3.64 × 10^{-19} molecules^{-1} s^{-1} cm^{-3} (2.98 × 10^{-19} molecules^{-1} s^{-1} cm^{-3}) in tropics, at daytime (at nighttime).

K_{eff} estimations obtained in this study are very low as well as those calculated by Cariolle et al. (2009), for the plume chemistry related to aircraft exhausts. In this previous work, K_{eff} varies from 1.0 to 4.2 × 10^{-18} molecules^{-1} s^{-1} cm^{-3} with a mean value close to 3 × 10^{-18} molecules^{-1} s^{-1} cm^{-3} depending on the NO$_x$ loading. The very low

value for K_{eff} point out that the plume parameterization implies a delay of the production of ozone at the large scale rather than its destruction within the plume.

3.2.5 The fractions of NO_x conversion to HNO_3 (β_1 and β_2)

The fractions β_1 and β_2 represent the NO_x conversion into HNO_3 within the plume at daytime and nighttime respectively. They were computed using the DSMACC chemical box model.

The β_1 coefficient was calculated for day conditions depending mainly on the OH concentration. The conversion of NO_x into HNO_3 at nighttime (β_2 coefficient) is related to the heterogeneous reaction of N_2O_5 and so depends on particles (aerosols and ice crystals) concentration and their lifetime. This is directly linked with the surface density and the radius of particles in the anvil region of thunderstorms, which is highly uncertain. We defined these values using in situ measurements. The surface area (S_T) and the radius (R) for aerosols are defined such as: $S_T = 0.28 \, \mathrm{m}^{-1}$ and $R = 1 \, \mu\mathrm{m}^{-1}$ (Huntrieser et al., 2002) and for ice, $S_T = 0.03 \, \mathrm{m}^{-1}$ and $R = 30 \, \mu\mathrm{m}^{-1}$ (Knollenberg et al., 1993). In addition, the reaction probabilities of NO_x on aerosols and ice crystals $\gamma_{N_2O_5}^{aerosols} = 0.02$ (Evans and Jacob, 2005) and $\gamma_{N_2O_5}^{ice} = 0.03$ (Sander et al., 2006), respectively, were used for our box model simulations. These values correspond to the probability that a N_2O_5 molecule impacting an aerosol or an ice crystal surface was subjected to react. The results for β_1 and β_2 coefficients are summarized in Table 4.

The estimate of β_1 fraction does not show significant variation neither between latitudes regions nor depending on NO_i. The minimum β_1 value is 1.34×10^{-4} for tropical regions and NO_i^{min}, and the maximum β_1 value is 1.88×10^{-4} for midlatitudes and NO_i^{max}. The study of production and destruction rates for day conditions taking into account all reactions pathways (not shown here) demonstrates that production of HNO_3 during the day is mainly determined by reaction of NO_3 with formaldehyde (HCHO) and acetaldehyde (CH_3CHO). Surprisingly, HNO_3 formation via the $NO_2 + OH$ reaction

seems to be less efficient. This result could be explained by the low initial concentrations of OH used for the DSMACC simulations and it is in agreement with the small β_1 values. Then, the averaged β_2 coefficient is higher by a factor 10 compared to β_1 with a minimum value of 0.24×10^{-3} in tropics for NO_i^{max} and a maximum estimate of 14.4×10^{-3} in midlatitudes for NO_i^{min}. The analysis of the production and the destruction rates for night conditions taking into account all reactions pathway shows that the predominant reaction in the HNO_3 evolution is $N_2O_5 + H_2O$ (or the heterogeneous reaction on the aerosols and ice crystals surface).

4 Results: CTM simulations

In this section, the effects of the lightning NO_x plume parameterization, i.e. the influence of sub-grid processes related to lightning emissions, on the NO_x and O_3 tropospheric distributions at large scale are evaluated. Then, the parameterization sensitivity to initial NO mixing ratio injected by lightning (NO_i), D_h, β_1 and β_2 coefficients is analyzed to quantify the variability of the results regarding the plume-in-grid parameter calculations.

4.1 Implementation of the LNO_x plume parameterization

The implementation of the lightning NO_x plume parameterization into the GEOS-Chem model requires specifying the system of continuity equations related to the plume chemistry solved at large scale by the model (Sect. 3.1.2, Eqs. 13–15). Lightning NO_x emissions calculated in each grid box (in molecules $cm^{-2} s^{-1}$) by the model are directly used to compute the injection rate I (s^{-1}) of NO at each chemical time step of the simulation. Then, we consider the following setup: $\alpha_{NO_x} = 1$ and $EI_{NO_x} = 1$, in order to represent the mixing ratio of the undiluted fraction of NO_x by the tracer (r_{LNO_x}). Furthermore, lightning produce only NO among NO_x species thus $E = 0$ in the Eq. (15).

Finally, the ratio $\overline{\frac{NO_2}{NO_x}}$ is the relative balance between NO and NO_2 in the diluted phase at large scale reproduced by the model.

4.2 Impact of LNO$_x$ emissions on the NO$_x$ and O$_3$ distributions

We perform a spin-up of six months (from July 2005 to January 2006) in order to obtain a steady state in the model after activation of the plume parameterization. Then simulations were run for the entire year 2006. The transport and the convection time steps are 15 min and the emissions and the chemical time steps are 30 min.

In the following, standard simulation refers to simulation with standard lightning NO$_x$ emissions i.e. instantaneously diluted in a grid cell, while modified simulation refers to simulation considering the plume parameterization and then sub-grid chemistry. Note that the modified simulation was run using mean values for the initial NO mixing ratio (NO$_i^{\text{mean, Midlats}}$ = 3.4 ppb and NO$_i^{\text{mean, Tropics}}$ = 10.2 ppb) and D_h = 15 m^2 s^{-1}. The Base Case (BC) experiment corresponds to the standard simulation minus the standard simulation without lightning NO$_x$ emissions. The P1 experiment corresponds to the modified simulation minus the standard simulation without lightning NO$_x$ emissions. The P2 experiment is the same as the P1 experiment but without considering the nitrification mechanism in the modified simulation (i.e. $\beta_1 = \beta_2 = 0$). In addition, sensitivity tests were performed for P1 defined by the modified simulation using the minimum and the maximum values for D_h, NO$_i$, β_1 and β_2 coefficients. All experiments are summarized in Table 5.

Lightning emissions rates and the associated LNO$_x$ tracer distributions are first discussed, then the effects of the implementation of the plume parameterization (P1) compared to the experiment without the plume-in-grid development (BC case) is presented.

4.2.1 Lightning emissions and LNO$_x$ tracer distributions

Figure 3 displays the geographical distributions of the 9 km lightning NO$_x$ emissions (a), the related LNO$_x$ tracer distributions (b) and the LNO$_x$ tracer zonal averaged (c) in January (top panels) and in July (bottom panels) reproduced by the CTM from the P1 experiment. These results are shown for an approximate detrainment level (9 km altitude) where the LNO$_x$ are the most concentrated. In January, the highest emissions of NO$_x$ from lightning ($4 - 6 \times 10^9$ molecules cm^{-2} s^{-1}) are located in the Southern Hemisphere around the tropics over West Australia and Central-South Africa. Also, the model gives low LNO$_x$ emissions ($< 3 \times 10^9$ molecules cm^{-2} s^{-1}) over South America and North America especially over the Gulf of Mexico. In July, the highest LNO$_x$ emissions ($4 - 6 \times 10^9$ molecules cm^{-2} s^{-1}) are calculated in the Northern Hemisphere over North America, North of India, Central Africa and Sahel. In addition, LNO$_x$ emissions are modeled over Europe and over East Asia but to a lesser extent ($< 2 \times 10^9$ molecules cm^{-2} s^{-1}).

The lightning NO$_x$ tracer introduced into the model represents the lightning NO$_x$ emissions affected by the transport and the exponential decay depending on the plume lifetime. Figure 3 shows that the tracer distribution is consistent with the lightning NO$_x$ emissions. However, it is important to note that the plume lifetime is a key factor in the evolution of the LNO$_x$ tracer mixing ratio. A long plume lifetime (several hours to several days) allows the intercontinental transport of LNO$_x$ plumes. The representation of the sub-grid chemistry and the transport of the non-linear chemistry effects related to the plume consideration becomes important for the chemistry of the regions located far downwind from source regions. According to its preliminary calculation (Sect. 3.2.3), the plume lifetime is longer in tropics (9 and 21.3 h for day and night conditions, respectively) than in midlatitudes (3 and 6 h, for day and night conditions, respectively). So, the LNO$_x$ tracer is characterized by a shorter lifetime as a plume over North America than over Central Africa and around the Sahel while the model simulated less important emissions over these regions especially in summer. In boreal winter, the mixing

ratio of the lightning NO_x tracer calculated by the model is about 0.21 ppb over Central and South Africa, 0.18 ppb over West Australia and 0.11 ppb over South America. In summer, the tracer mixing ratio is simulated as 0.21, 0.32 and 0.16 ppb over Central Africa, North India and North America, respectively. The lightning NO_x tracer is mainly reproduced at altitudes where lightning NO_x are produced and detrained (in the upper troposphere) as shown in panels (c) in Fig. 3.

4.2.2 Impact of lightning on NO_x and O_3 distributions with the plume parameterization

The difference between P1 and BC experiments (P1 – BC) was calculated in order to quantify the changes on NO_x and O_3 mixing ratios at large scale implied by the implementation of the plume-in-grid parameterization into GEOS-Chem. Figures 4 and 5 display the geographical distributions of the NO_x, HNO_3, PAN and O_3 absolute changes (in ppb) in January and in July, respectively. The 9 km altitude level was chosen because of the most significant variations at this altitude compared to the rest of the troposphere.

In boreal winter, LNO_x plume chemistry leads to a maximum decrease at large scale over regions of emissions of 120 ppt for NO_x and a decrease of 68 ppt for HNO_3 and 16 ppt for PAN over Central and South Africa. These variations are associated with a maximum O_3 decrease of 2.8 ppb over regions of emissions. A similar NO_x, HNO_3, PAN and O_3 reduction is obtained in other areas of high LNO_x emissions (i.e. over West Australia and South America). Downwind of LNO_x emissions the opposite effect is observed for NO_x and HNO_3 species with maximum increase of 40 ppt for NO_x and 13.5 ppt for HNO_3 observed over South Atlantic and Indian Ocean. Generally, PAN still decreases over oceans but in a lesser extent compared to regions of LNO_x emissions, with a maximum reduction of 9 ppt. O_3 response is a maximum increase of 1.13 ppb around area where the transport is effective and especially over the oceans. In summer, maximum decreases of 140 ppt for NO_x and 60 ppt for HNO_3 and 24 ppt for PAN are calculated by the CTM leading to a maximum O_3 decrease of 2.4 ppb over Cen-

tral Africa (reduction also observed over North America and North India). Downwind of lightning emissions, increase of NO_x and HNO_3 is observed with a maximum value of 30 and 38 ppt, respectively. PAN reservoir species also still decreases slightly downwind with 2 ppt changes. Finally, that leads to maximum O_3 increase of 0.7 ppb.

Note that the production of PAN is limited by the supply of NO_x or non-methane volatil organic compounds (NMVOCs). Above continental lightning sources regions, NMVOCs are uplifted by deep convection but with lower NO_x due to the activation of the plume parameterization. That implies a less efficient PAN production in these regions. Downwind of lightning sources regions (oceanic regions), NO_x increases because of the LNO_x transport in plume form but there is less NMVOCs available to produce PAN. Therefore, the production is limited leading to an overall lower PAN production in P1.

In order to provide a full overview of the effects of the plume parameterization, the relative difference between the P1 and BC experiments (i.e. (P1–BC) /BC) was calculated integrated throughout the troposphere. Figures 6 and 7 show zonal averaged of NO_x (upper panels) and O_3 (bottom panels) relative changes (in %) integrated throughout the troposphere for regions of interest for January and July, respectively. During boreal winter, the highest NO_x (O_3) decreases of 10 % (5 %) in West Australia, then 20 % (6 %) in Central Africa are calculated. These negative variations are mainly calculated between 400 hPa and the tropopause level for NO_x and ozone. South America is characterized by a decrease of 20 % of the nitrogen oxides and 1 % of ozone. Over this region, variations are significant in the entire troposphere for both species. In contrast to the continent decrease, NO_x increase is observed over the major part of South Atlantic and Indian Ocean with 14 and 20 % maximum, respectively. The O_3 response in an increase of 1 % near the tropopause and it becomes higher close to the surface of about 4 %. In summer, there is a NO_x (O_3) decrease of 25 % (8 %) over Central Africa, 20 % (2 %) over North India, and 5 % (0.5 %) over North America. Also, South Atlantic and Indian Ocean (located downwind of lightning NO_x emissions) are characterized by a maximum increase of 18 % for NO_x and 2 % for O_3.

As a result, the sub-grid chemistry associated to the LNO_x emissions implies (i) a decrease of the nitrogen oxides and ozone mixing ratios at large scale over regions characterized by intense lightning emissions and (ii) an increase of these species downwind of emissions. Especially the plume parameterization related to the lightning NO_x leads to:

1. Significant effects on NO_x mixing ratio (±20 %): these effects on nitrogen oxides are important because NO_x is the first criterion which is constrained in a CTM in order to determine the global LNO_x production ($6\,\mathrm{Tg\,N\,yr^{-1}}$ in the GEOS-Chem model).

2. Lower effects on O_3 mixing ratio (±5 %): these limited impacts on ozone could be explained by compensatory effect of the NO_y species (mainly conversion of NO_x into (i) HNO_3 within the plume or (ii) PAN).

The effects of the plume parameterization are simulated over the entire troposphere mainly for ozone. Indeed, the spreading of effects on ozone to the lower free troposphere is related to the subsidence areas of the Walker circulation. These regions are characterized by accumulation and creation of ozone for low altitude levels. Nevertheless, the maximum NO_x and O_3 variations are calculated for altitude levels associated with a mean detrainment level. The realistic representation of the sub-grid processes (P1 experiment) related to the LNO_x plume is in contrast with the simplified instantaneous dilution in the grid cell of the lightning NO_x emissions (BC experiment).

The plume approach allows the conversion of NO_x into HNO_3 during the plume lifetime. In addition, the high NO_x concentration within the plume (much higher than the background content) leads to the O_3 titration and more generally to the O_x destruction within the plume. The most important impact of the plume parameterization is the transport of the LNO_x emissions as a plume and the transport of the associated nonlinear chemistry effects leading to a delay of the O_3 production at large scale. In other words, O_3 is less produced over the regions with intense lightning NO_x emissions than downwind of LNO_x emissions by photochemical reactions from NO_x.

4.3 Plume sensitivity to the estimated uncertainties of parameter calculations

4.3.1 The Atmospheric dynamical conditions and the initial NO mixing ratio injected by lightning

The impact of (i) the diffusion properties of the atmosphere (D_h) and (ii) the initial NO mixing ratio injected by lightning (NO_i) are analyzed. D_h and NO_i are the two key parameters in the determination of the physical and chemical characteristics of the plume. The modified simulation characterizing the P1 experiment was run for the ranges of the horizontal diffusion coefficients and the initial NO mixing ratio injected by lightning. It is important to note that for these sensitivity tests, β_1 and β_2 coefficients remain constant using their mean values. τ and K_{eff} values related to these simulations are those previously calculated (Sect. 3) and summarized in Tables 2 and 3. Figure 8 displays τ (upper panels) and K_{eff} (bottom panels) variations depending on D_h and NO_i. As expected, the strongest the horizontal diffusion is the most efficient the dispersion of the plume is. In both, midlatitudes and tropics, τ decreases when D_h becomes larger. In addition, τ increases with the initial NO mixing ratio injected by lightning. In contrary, K_{eff} increases with D_h coefficient in the two regions of the globe.

The variability of NO_x and O_3 mixing ratios around the mean value for regions and seasons depending on the known uncertainties associated with parameter calculations have been quantified. Figure 9 shows the intervals of variability of NO_x and O_3 (ΔNO_x and ΔO_3, respectively) at 9 km altitude reproduced by GEOS-Chem depending on D_h and on the initial NO mixing ratio (NO_i). Note that for the sake of readability, the scale of NO_x and O_3 changes differs by region. Results are also summarized in Table 6.

We chose representative continental areas such as Florida and Congo, which correspond to regions characterized by intense electrical activity for midlatitudes and tropics, respectively. North and South Atlantic were selected to represent regions downwind of NO_x emissions, for mid-latitude and tropic variations, respectively. The highest ranges of NO_x and O_3 changes are obtained for continental tropical regions with ΔNO_x [−33.1; +29.7] ppt and ΔO_3 [−1.56; +2.16] ppb, in January, and ΔNO_x [−14.3;

+21] ppt and ΔO_3 [−1.18; +1.93] ppb, in July. The largest variation range associated with the tropical continents could be explained by the largest difference on parameter values defining the plume in this region (especially NO$_i$). The smallest intervals are observed over continental mid-latitude regions for winter with ΔNO_x [−1.7; +1.8] ppt and ΔO_3 [−0.16; +0.72] ppb and over oceanic tropical regions in summer such as ΔNO_x [−11.5; +2.6] ppt and ΔO_3 [−0.14; +0.92] ppb. As a result, the variability of NO$_x$ and O$_3$ species to the parameter uncertainties is a few ppt for NO$_x$ and less than 2 ppb for O$_3$.

4.3.2 Coefficients related to the nitrification mechanism (β_1 and β_2)

In order to estimate the variability of the NO$_x$ and O$_3$ mixing ratios related to the uncertainties on β_1 and β_2 fractions (Table 7), the difference between P1 experiment using β_1 and β_2 mean values and P1 experiment using minimum and maximum β_1 and β_2 coefficients has been calculated. This implies that τ and K_{eff} are constant.

In January, the highest variability on NO$_x$ mixing ratio is ΔNO_x [−2.3; +0.9] ×10^{-2} ppt over continental tropical regions and ΔO_3 [−10; +11] ×10^{-4} ppb over tropical ocean on O$_3$, while mid-latitude oceanic areas show minimum ranges on NO$_x$ and O$_3$ with ΔNO_x ± 2.3 × 10^{-2} ppt associated with ΔO_3 [−9; +4] ×10^{-4} ppb. In July, the maximum ranges are calculated over oceans in midlatitudes for NO$_x$ such as ΔNO_x [−21.1; +6.6] ×10^{-2} ppt and in tropics for O$_3$ with ΔO_3 [−30; −2] ×10^{-4} ppb. Finally, the smallest intervals, ΔNO_x [−0.9; −0.4] ×10^{-2} ppt and ΔO_3 [−24; −6] ×10^{-4} ppb, are simulated for tropical ocean and mid-latitude continent, respectively.

In addition, the impact of the nitrification mechanism was assessed comparing the P1 experiment using mean β_1 and β_2 values and P2 experiment for which $\beta_1 = \beta_2 = 0$. As a result, taking into account NO$_x$ conversion into HNO$_3$ using the mean β fractions calculated in this study does not imply strong changes in NO$_x$ and O$_3$ distributions ($\Delta NO_x < 10^{-4}$ ppb and $\Delta O_3 < 10^{-2}$ ppb).

In the case of significant values of β fractions, the rate of the nitrification mechanism should imply a delay of the O_3 formation from the NO_x in the plume because of the NO_x storage into HNO_3. On the other hand, HNO_3 is considered as a one of the main sink for NO_x species undergoing wet deposition and seemingly limiting their affect on global ozone.

The sensitivity tests point out the limited effect of the NO_x conversion to HNO_3 within the plume using our β_1 and β_2 estimates. The variability on NO_x and O_3 mixing ratios related to β coefficients is about a few ppt. That could be explained by small β values resulting from our estimate unlike Cariolle et al. (2009) highlighted the significant influence of these fractions in the case of aircraft NO_x emissions. In our study, we can easily suppose that the increase of the β_1 and β_2 coefficients should be in agreement with the work of Cooper et al. (2014) in reducing the underestimation of HNO_3 production induced by NO_x emissions from lightning. Further estimates of β should be realized using future observations in cloud anvil of primary species, aerosols and particules needed for NO_x conversion at daytime and nighttime to improve the determination of these parameters. β_1 coefficient is particularly dependent on the HO_x radicals, which could vary significantly within the cloud anvil in part because of the transport of peroxides from the lower troposphere by convective uplift (Wennberg et al., 1998). Then, the determination of β_2, corresponding to the NO_x conversion fraction into HNO_3 via N_2O_5 formation during nighttime is considerably dependent on (i) the estimate of aerosols and ice crystal concentration and their lifetime within the cloud anvil which is highly uncertain according to measurement campaigns and (ii) on the reaction probability on aerosols $\gamma_{N_2O_5}^{aerosol}$ and ice crystals $\gamma_{N_2O_5}^{ice}$ from laboratory studies extrapolations.

According to results presented in this section, sensitivity tests show the predominance of the initial NO mixing ratio injected by lightning (NO_i) and the diffusion properties of the atmosphere (D_h) in the variability of the NO_x and O_3 mixing ratios around the mean value in response to the plume-in-grid parameterization in the CTM. In winter, the NO_x and O_3 variability is the highest for continental regions in the tropics and the smallest variability is calculated for midlatitudes. In summer, the most important

variability of NO_x and O_3 is simulated in tropics over regions characterized by intense LNO_x emissions while the least significant sensitivity is obtained still in the tropics but downwind of emissions (mainly over oceans).

5   Conclusions

For the first time, a realistic lightning NO_x chemistry is implemented as a plume parameterization into a global chemical transport model. The key parameters characterizing the lightning-related plume were estimated depending on two main criteria, i.e. the NO mixing ratio injected by lightning (NO_i) and the atmospheric diffusion coefficient (D_h).

According to the NO_i and D_h ranges, the plume lifetime (τ) and the effective reaction rate constant (K_{eff}) for NO_x-O_3 chemical interactions were estimated as follow:

- $\tau = [0.01; 68.5]\,h$;

- $K_{eff} = [0.77; 23] \times 10^{-19}\,molecules^{-1}\,s^{-1}\,cm^{-3}$.

Also, for the conditions defined by NO_i^{mean} and $D_h = 15\,m^2\,s^{-1}$:

- τ is 3 (6) h in midlatitudes and 9 (21.3) h in tropics at daytime (nighttime);

- K_{eff} is $5.49 \times 10^{-19}\,molecules^{-1}\,s^{-1}\,cm^{-3}$ ($4.55 \times 10^{-19}\,molecules^{-1}\,s^{-1}\,cm^{-3}$) in midlatitudes and $3.64 \times 10^{-19}\,molecules^{-1}\,s^{-1}\,cm^{-3}$ ($2.98 \times 10^{-19}\,molecules^{-1}\,s^{-1}\,cm^{-3}$) in tropics at daytime (nighttime).

Finally, the fractions of NO_x conversion into HNO_3 within the plume are $\beta_1 = [1.34; 1.88] \times 10^{-4}$, and $\beta_2 = [0.24; 14.4] \times 10^{-3}$ for day and night conditions respectively.

GEOS-Chem simulations performed using mean value for NO_i and $D_h = 15\,m^2\,s^{-1}$ reveal nitrogen species and ozone changes compared to the instantaneous dilution. A decrease of NO_x and O_3 mixing ratios at large scale over the regions of strong LNO_x emissions is observed mainly in the Northern Hemisphere in summer and in

the Southern Hemisphere in winter. In the troposphere, maximum decrease of 20 % (6 %) in January and 25 % (8 %) in July for NO_x (O_3), are found over Central Africa. In contrast, an increase of NO_x (O_3) downwind of emissions is simulated of 20 % (4 %) in January and 18 % (2 %) in July. The LNO_x plume parameterization allows the transport
5 of the effects on the non-linear chemistry occurring within the plume and the conversion of NO_x to the nitrogen reservoir species (mainly HNO_3). However, the most significant impact is the transport of the LNO_x as a plume. That implies a delay of (i) the NO_x release into the point grid and (ii) ozone production from NO_x emitted by lightning flashes corresponding to the decrease of the NO_x and O_3 mixing ratios at large scale
10 over regions of emissions and their increase over transport pathway.

The variability of the NO_x and O_3 mixing ratios around the mean value depending on the known uncertainties on the plume physics and chemistry key parameters has been estimated. The highest sensitivity is obtained for continental tropical regions with ΔNO_x [−33.1; +29.7] ppt and ΔO_3 [−1.56; +2.16] ppb, in January, and ΔNO_x [−14.3; +21] ppt
15 and ΔO_3 [−1.18; +1.93] ppb, in July. Concerning β_1 and β_2 fractions, the highest variability depending on the fraction uncertainties for NO_x is ΔNO_x[−2.3; +0.9] × 10^{-2} ppt over continental tropical regions, and ΔO_3 [−10; +11] ×10^{-4} ppb for O_3 over tropical ocean in January. In summer, the maximum ranges are calculated over oceans in midlatitudes for NO_x such as ΔNO_x[−21.1; +6.6] × 10^{-2} ppt and in tropics for O_3 with ΔO_3
20 [−30; −2] ×10^{-4} ppb. Accordingly, parameters leading to the highest uncertainties on results and which drive the plume-in-grid parameterization are NO_i and D_h.

This study demonstrates the importance to consider the plume-in-grid chemistry related to the lightning NO_x emissions occurring at smaller scale for global calculations. Taking into account the plume dilution into the background atmosphere in time and
25 space with the transport of the NO_x and O_3 non-linear chemistry effects and the conversion of NO_x into HNO_3 reservoir species, implies more realistic NO_x and O_3 concentrations in CTM. The plume-in-grid approach, by allowing realistic sub-grid chemistry will allow improving the different steps in the lightning NO_x emissions modeling such as the convection process, the calculation of the NO molecules produced by lightning

discharges depending on regions according to recent and future satellite observations, and also processes like HNO_3 scavenging and HNO_3 uptake by ice crystals.

References

Amos, H. M., Jacob, D. J., Holmes, C. D., Fisher, J. A., Wang, Q., Yantosca, R. M., Corbitt, E. S., Galarneau, E., Rutter, A. P., Gustin, M. S., Steffen, A., Schauer, J. J., Graydon, J. A., Louis, V. L. St., Talbot, R. W., Edgerton, E. S., Zhang, Y., and Sunderland, E. M.: Gas-particle partitioning of atmospheric Hg(II) and its effect on global mercury deposition, Atmos. Chem. Phys., 12, 591–603, doi:10.5194/acp-12-591-2012, 2012. 34096

Aumont, B.: Modélisation de la chimie troposphérique, Université Paris 12 – UFR de Sciences et Technologie, HDR report, Val de Marne, 2005. 34106

Banerjee, A., Archibald, A. T., Maycock, A. C., Telford, P., Abraham, N. L., Yang, X., Braesicke, P., and Pyle, J. A.: Lightning NO_x, a key chemistry–climate interaction: impacts of future climate change and consequences for tropospheric oxidising capacity, Atmos. Chem. Phys., 14, 9871–9881, doi:10.5194/acp-14-9871-2014, 2014. 34093

Bechtold, P., Bazile, E., Guichard, F., Mascart, P., and Richard, E.: A mass-flux convection scheme for regional and global models, Q. J. Roy. Meteor. Soc., 127, 869–886, 2000. 34097

Bey, I., Jacob, D. J., Yantosca, R. M., Logan, J. A., Field, B. D., Fiore, A. M., Li, Q., Liu, H. Y., Mickley, L. J., and Schultz, M. G.: Global modeling of tropospheric chemistry with assimilated meteorology: model description and evaluation, J. Geophys. Res., 106, 23073–23095, 2001. 34095, 34096

Bian, H. and Prather, M. J.: Fast-J2: Accurate simulation of stratospheric photolysis in global chemical models, J. Atmos. Chem., 41, 281–296, 2002. 34096

Cariolle, D., Caro, D., Paoli, R., Hauglustaine, D. A., Cuénot, B., Cozic, A., and Paugam, R.: Parametrization of plume chemistry into large-scale atmospheric models: application to

aicraft NO$_x$ emissions, J. Geophys. Res., 114, D19302, doi:10.1029/2009JD011873, 2009. 34098, 34100, 34101, 34102, 34103, 34108, 34121

Choi, Y., Kim, J., Eldering, A., Osterman, G., Yung, Y. L., Gu, Y., and Liou, K. N.: Lightning and anthropogenic NO$_x$ sources over the United States and the western North Atlantic Ocean: impact on OLR and radiative effects, Geophys. Res. Lett., 36, L17806, doi:10.1029/2009GL039381, 2009. 34093

Christian, H. J., Blakeslee, R. J., Boccippio, D. J., Boeck, W. L., Buechler, D. E., Driscoll, K. T., Goodman, S. J., Hall, J. M., Koshak, W. J., Mach, D. M., and Stewart, M. F.: Global frequency and distribution of lightning as observed from space by the Optical Transient Detector, J. Geophys. Res., 108, 4005, doi:10.1029/2002JD002347, 2003. 34093, 34109

Cohard, J.-M. and Pinty, J. P.: A comprehensive two-moment warm microphysical bulk scheme, I: Description and tests, Q. J. Roy. Meteor. Soc., 126, 1815–1842, 2000. 34097

Cooper, M., Martin, R. V., Wespes, C., Coheur, P.-F., Clerbaux, C., and Murray L. T.: Tropospheric nitric acid columns from the IASI satellite instrument interpreted with a chemical transport model: implications for parameterizations of nitric oxide production by lightning, J. Geophys. Res., 119, 10068–10079, 2014. 34094, 34121

Cuxart, J., Bougeault, P., and Redelsperger, J. L.: A turbulence scheme allowing for mesoscale and large-eddy simulations, Q. J. Roy. Meteor. Soc., 126, 1–30, 1999. 34097, 34107

Damian, V., Sandu, A., Damian, M., Potra, F., and Camichael, G. R.: The kinetic preprocessor KPP – a software environment for solving chemical kinectics, Comput. Chem. Eng., 26, 1567–1579, 2002. 34097

Dye, J. E., Ridley, B. A., Skamarock, W., Barth, M., and Venticinque, M.: An overview of the Stratospheric–Tropospheric experiment: radiation, aerosols, and ozone (STERAO)-Deep convection experiment with results for the July 10, 1996 storm, J. Geophys. Res., 105, 10023–10045, 2000. 34101, 34110

Emmerson, K. M. and Evans, M. J.: Comparison of tropospheric gas-phase chemistry schemes for use within global models, Atmos. Chem. Phys., 9, 1831–1845, doi:10.5194/acp-9-1831-2009, 2009. 34097

Evans, M. J. and Jacob, D. J.: Impact of new laboratory studies of N$_2$O$_5$ hydrolysis on global model budgets of tropospheric nitrogen oxides, ozone, and OH, Geophys. Res. Lett., 32, L09813, doi:10.1029/2005GL022469, 2005. 34112

Modeling lightning-NO$_x$ chemistry at sub-grid scale

A. Gressent et al.

Title Page

Abstract | Introduction

Conclusions | References

Tables | Figures

|◄ | ►|

◄ | ►

Back | Close

Full Screen / Esc

Printer-friendly Version

Interactive Discussion

Gregory, D., Morcrette, J.-J., Jakob, C., Beljaars, A. C. M., and Stockdale, T.: Revision of convection, radiation and cloud schemes in the ECMWF Integrated Forecasting System, Q. J. Roy. Meteor. Soc., 126, 1685–1710, 2000. 34097

Grewe, V.: Impact of climate variability on tropospheric ozone, Sci. Total Environ., 374, 167–181, 2007. 34093

Guenther, A. B., Jiang, X., Heald, C. L., Sakulyanontvittaya, T., Duhl, T., Emmons, L. K., and Wang, X.: The Model of Emissions of Gases and Aerosols from Nature version 2.1 (MEGAN2.1): an extended and updated framework for modeling biogenic emissions, Geosci. Model Dev., 5, 1471–1492, doi:10.5194/gmd-5-1471-2012, 2012. 34096

Hauglustaine, D., Emmons, L., Newchurch, M., Brasseur, G., Takao, T., Matsubara, K., Johnson, J., Ridley, B., Stith, J., and Dye, J.: On the role of lightning NO_x in the formation of tropospheric ozone plumes: a global model perspective, J. Atmos. Chem., 38, 277–294, 2001. 34093

Hauglustaine, D. A., Granier, C., and Brasseur, G. P.: Impact of present aircraft emissions of nitrogen oxides on troposheric ozone and climate forcing, Geophys. Res. Lett., 21, 2031–2034, 1994. 34093

Hudman, R.C., Jacob, D. J., Turquety, S., Leibensperger, E. M., Murray, L. T., Wu, S., Gilliland, A. B., Avery, M., Bertram, T. H., Brune, W., Coben, R. C., Dibb, J. E., Flocke, F. M., Fried, A., Holloway, J., Neumann, J. A., Orville, R., Perning, A., Ren, X., Sachse, G. W., Singh, H. B., Swanson, A., and Wooldridge, P. J.: Surface and lightning sources of nitrogen oxides over the United States: magnitudes, chemical evolution, and outflow, J. Geophys. Res., 112, D12S05, doi:10.1029/2006JD007912, 2007. 34093, 34094

Huntrieser, H., Schlager, H., Feigl, C., and Höller, H.: Transport and production of NO_x in electrified thunderstorms: survey of previous studies and new observations at midlatitudes, J. Geophys. Res., 103, 28247–28264, 1998. 34110

Huntrieser, H., Feigl, C., Schlager, H., Schröder, F., Gerbig, C., and van Velthoven, P.: Airborne measurements of NO_x, tracer species, and small particles during the European Lightning Nitrogen Oxides Experiment, J. Geophys. Res., 107, 4113, doi:10.1029/2000JD000209, 2002. 34101, 34110, 34112

Huszar, P., Cariolle, D., Paoli, R., Halenka, T., Belda, M., Schlager, H., Miksovsky, J., and Pisoft, P.: Modeling the regional impact of ship emissions on NO_x and ozone levels over the Eastern Atlantic and Western Europe using ship plume parameterization, Atmos. Chem. Phys., 10, 6645–6660, doi:10.5194/acp-10-6645-2010, 2010. 34094, 34098

Title Page

Abstract | Introduction

Conclusions | References

Tables | Figures

|◀ | ▶|

◀ | ▶

Back | Close

Full Screen / Esc

Printer-friendly Version

Interactive Discussion

Jacobson, M. Z. and Turco, R. P.: SMVGEAR: a sparse-matrix, vectorized gear code for atmospheric models, Atmos. Environ., 28, 273–284, 1994. 34096

Jaeglé, L., Jacob, D. J., Brune, W. H., Tan, D., Faloona, I. C., Weinheimer, A. J., Ridley, B. A., Campos, T. L., and Sachse, G. W.: Soucres and chemistry of NO_x in the upper troposphere over the United Sates, Geophys. Res. Lett., 25, 1705–1708, 1998. 34101

Jenkin, M. E., Saunders, S. M., and Pilling, M. J.: The tropospheric degradation of volatile organic compounds: a protocol for mechanism development, Atmos. Environ., 31, 81–104, 1997. 34097

Klemp, J. B. and Wilhelmson, R. B.: The simulation of three-dimensional convective storm dynamics, J. Atmos. Sci., 35, 1070–1096, 1978. 34107

Knollenberg, R. G.: Measurements of the growth of the ice budget in a persisting contrail, J. Atmos. Sci., 29, 1367–1374, 1972. 34108

Knollenberg, R. G., Kelly, K., and Wilson, J. C.: Measurements of high number densities of ice crystals in the tops of tropical cumulonimbus, J. Geophys. Res., 98, 8639–8664, 1993. 34112

Labrador, L. J., von Kuhlmann, R., and Lawrence, M. G.: Strong sensitivity of the global mean OH concentration and te tropospheric oxidizing efficiency to the source of NO_x from lightning, Geophys. Res. Lett., 31, L06102, doi:10.1029/2003GL019229, 2004. 34093

Lafore, J. P., Stein, J., Asencio, N., Bougeault, P., Ducrocq, V., Duron, J., Fischer, C., Héreil, P., Mascart, P., Masson, V., Pinty, J. P., Redelsperger, J. L., Richard, E., and Vilà-Guerau de Arellano, J.: The Meso-NH Atmospheric Simulation System. Part I: adiabatic formulation and control simulations, Ann. Geophys., 16, 90–109, doi:10.1007/s00585-997-0090-6, 1998. 34097

Lange, L., Hoor, P., Helas, G., Fischer, H., Brunner, D., Scheeren, B., Williams, J., Wong, S., Wohlfrom, K.-H., Arnold, F., Ström, J., Krejci, R., Lelieveld, J., and Andreae, M. O.: Detection of lightning-produced NO in the midlatitude upper troposphere during STREAM 1998, J. Geophys. Res., 106, 27777–27785, 2001. 34110

Lascaux, F., Richard, E., and Pinty, J. P.: Numerical simulations of three different MAP IOPs and the associated microphysical processes, Q. J. Roy. Meteor. Soc., 132, 1907–1926, 2006. 34097

Lin, J.-T. and McElroy, M. B.: Impacts of boundary layer mixing on pollutant vertical profiles in the lower troposphere: implications to satellite remote sensing, Atmos. Environ., 44, 1726–1739, 2010. 34096

Title Page

Abstract | Introduction

Conclusions | References

Tables | Figures

|◄ | ►|

◄ | ►

Back | Close

Full Screen / Esc

Printer-friendly Version

Interactive Discussion

Lin, S.-J. and Rood, R. B.: Multidimensional flux-form semi-lagrangian transport scheme, Mon. Weather Rev., 124, 2046–2070, 1996. 34096

Lin, X., Trainer, M., and Liu, S. C.: On the nonlinearity of the tropospheric ozone production, J. Geophys. Res., 93, 15879–15888, 1988. 34094

Liu, H., Jacob, D. J., Rey, I., and Yantosca, R. M.: Constraints from ^{210}Pb and ^{7}Be on wet deposition and transport in a global three-dimensional chemical tracer model driven by assimilated meteorological fields, J. Geophys. Res., 106, 12109–12128, 2001. 34096

Lobert, J. M., Keene, W. C., Logan, J. A., and Yevich, R.: Global chlorine emissions from biomass burning: reactive chlorine emissions inventory, J. Geophys. Res., 104, 8373–8389, 1999. 34096

Madronich, S. and Flocke, S.: Environmental Photochemistry, Springer Berlin Heidelberg, Germany, ISBN: 9783662147351, doi:10.1007/978-3-540-69044-3, 1999. 34097

Martin, R. V., Jacob, D. J., Logan, J. A., Bey, I., Yantosca, R. M., Staudt, A. C., Li, Q., Fiore, A. M., Duncan, B. N., and Liu, H.: Interpretation of TOMS observations of tropical tropospheric ozone with a global model and in situ observations, J. Geophys. Res., 107, 4351, doi:10.1029/2001JD001480, 2002. 34096

Martin, R. V., Sauvage, B., Folkins, I., Sioris, C. E., Boone, C., Bernath, P., and Ziemke, J.: Space-based constraints on the production of nitric oxide by lightning, J. Geophys. Res., 112, D09309, doi:10.1029/2006JD007831, 2007. 34093, 34094, 34097

Monks, P. S.: Gas-phase radical chemistry in the tropopshere, Chem. Soc. Rev., 34, 376–395, 2005. 34105

Moorthi, S. and Suarez, M. J.: Relaxed Arakawa-Schubert: a parameterization of moist convection for general circulation models, Mon. Weather Rev., 120, 978–1002, 1991. 34096

Murray, L. T., Jacob, D. J., Logan, J. A., Hudman, R. C., and Koshak, J.: Optimized regional and interannual variability of lightning in a global chemical transport model constrained by LIS/OTD satellite data, J. Geophys. Res., 117, D20307, doi:10.1029/2012JD017934, 2012. 34093, 34097

Olivier, J. G. J.: Recent trends in global greenhouse gas emissions: regional trends and spatial distribution of key sources, Environment Sciences, 2, 81–89, 2005. 34096

Ott, L. E., Pickering, K. E., Stenchikov, G. L., Allen, D. J., DeCaria, A. J., Ridley, B., Lin, R. F., Lang, S., and Tao, W.-K.: Production of lightning NO$_x$ and its vertical distribution calculated from three-dimensional cloud-scale chemical transport model simulations, J. Geophys. Res., 115, D04301, doi:10.1029/2009JD011880, 2010. 34096, 34100

Paoli, R., Cariolle, D., and Sausen, R.: Review of effective emissions modeling and computation, Geosci. Model Dev., 4, 643–667, doi:10.5194/gmd-4-643-2011, 2011. 34098

Pickering, K. E., Thompson, A. M., Dickerson, R. R., Luke, W. T., MacNamara, D. P., Greenberg, J. P., and Zimmerman, P. R.: Model calculations of tropospheric ozone production potentiel following observed convective events, J. Geophys. Res., 95, 14049–14062, 1990. 34093

Pickering, K. E., Wang, Y., Tao, W.-K., Price, C., and Müller, J.-F.: Vertical distributions of lightning NO$_x$ for use in regional and global chemical transport models, J. Geophys. Res., 103, 31203–31216, 1998. 34094, 34096

Pinty, J. P. and Jabouille, P.: A mixed-phase cloud parameterization for use in a mesoscale non-hydrostatic model: simulations of a squall line and of orographic precipitation, American Meteorological Society, Conference on cloud physics, 17–21 August 1998, Everett, WA, USA, 217–220, 1999. 34097

Price, C. and Rind, D.: A simple lightning parameterization for calculating global lightning distributions, J. Geophys. Res., 97, 9919–9933, 1992. 34093, 34096

Price, C. and Rind, D.: Possible implications of global climate change on global lightning distributions and frequencies, J. Geophys. Res., 99, 10823–10831, 1994. 34096

Sander, S. P., Friedl, R. R., Golden, D. M., Kurylo, M. J., Moortgat, G. K., Wine P. H., Ravishankara, A. R., Kolb, C. E., Molina, M. J., Finlayson-Pitts, B. J., Huie, R. E., and Orkin, V. L.: Chemical Kinetics and Photochemical Data for Use in Atmosperic Studies, Evaluation Number 15, Tech. rep., NASA, Jet Propulsion Laboratory, California Institute of Technology, Pasadena, California, USA, 2006. 34112

Saunders, S. M., Jenkin, M. E., Derwent, R. G., and Pilling, M. J.: Protocol for the development of the Master Chemical Mechanism, MCM v3 (Part A): tropospheric degradation of non-aromatic volatile organic compounds, Atmos. Chem. Phys., 3, 161–180, doi:10.5194/acp-3-161-2003, 2003. 34098

Sauvage, B., Martin, R. V., van Donkelaa, A., and Ziemke, J. R.: Quantification of the factors controlling tropical tropopsheric ozone and the South Atlantic maximum, J. Geophys. Res., 112, D11309, doi:10.1029/2006JD008008, 2007a. 34093

Sauvage, B., Martin, R. V., van Donkelaar, A., Liu, X., Chance, K., Jaeglé, L., Palmer, P. I., Wu, S., and Fu, T.-M.: Remote sensed and in situ constraints on processes affecting tropical tropospheric ozone, Atmos. Chem. Phys., 7, 815–838, doi:10.5194/acp-7-815-2007, 2007b. 34093, 34096

Title Page

Abstract | Introduction

Conclusions | References

Tables | Figures

|◄ | ►|

◄ | ►

Back | Close

Full Screen / Esc

Printer-friendly Version

Interactive Discussion

Schumann, U. and Huntrieser, H.: The global lightning-induced nitrogen oxides source, Atmos. Chem. Phys., 7, 3823–3907, doi:10.5194/acp-7-3823-2007, 2007. 34093

Stith, J., Dye, J., Ridley, B., Laroche, P., Defer, E., Hübler, G., Zerr, R., and Venticinque, M.: NO signatures from lightning flashes, J. Geophys. Res., 104, 16081–16089, 1999. 34110

5 Stockwell, D. Z., Giannakopoulos, C., Plantevin, P. H., Carver, G. D., Chipperfield, M. P., Law, K. S., Pyle, J. A., Shallcross, D. E., and Wang, K. Y.: Modelling NO_x from lightning and its impact on global chemical fields, Atmos. Environ., 33, 4477–4493, 1999. 34093

Streets, D. G., Zhang, Q., Wang, L., He, K., Hao, J., Wu, Y., Tang, Y., and Carmichael, G. R.: Revisting China's CO emissions after the Transport and Chemical evolution over the Pacific (TRACE-P) mission: synthesis of inventories, atmospheric modeling, and observations, J. Geophys. Res., 111, D14306, doi:10.1029/2006JD007118, 2006. 34096

Tost, H., Jöckel, P., and Lelieveld, J.: Lightning and convection parameterisations – uncertainties in global modelling, Atmos. Chem. Phys., 7, 4553–4568, doi:10.5194/acp-7-4553-2007, 2007. 34093

15 Trier, S. B. and Sharman, R. D.: Convection-permitting simulations of the environment supporting widespread turbulence within the upper-level outflow of a mesoscale convective system, American Meteorological Society, 137, 1972–1990, 2008. 34107

Tulet, P., Crassier, V., Solmon, F., Guedalia, D., and Rosset, R.: Description of the mesoscale nonhydrostatic chemistry model and application to a transboundary pollution episode between northern France and southern England, J. Geophys. Res., 108, 4021, doi:10.1029/2000JD000301, 2003. 34097

Tulet, P., Grini, A., Griffin, R. J., and Petitcol, S.: ORILAM-SOA: A compitationnaly efficient model for predicting secondary organic aerosols in three-dimensional atmospheric models, J. Geophys. Res., 111, D23208, doi:10.1029/2006JD007152, 2006. 34097

25 Wang, Q., Jacob, D. J., Fisher, J. A., Mao, J., Leibensperger, E. M., Carouge, C. C., Le Sager, P., Kondo, Y., Jimenez, J. L., Cubison, M. J., and Doherty, S. J.: Sources of carbonaceous aerosols and deposited black carbon in the Arctic in winter-spring: implications for radiative forcing, Atmos. Chem. Phys., 11, 12453–12473, doi:10.5194/acp-11-12453-2011, 2011. 34096

30 Wang, Y., Jacob, D. J., and Logan, J. A.: Global simulation of tropospheric O_3-NO_x-hydrocarbon chemistry – 1. Model formulation, J. Geophys. Res., 103, 10713–10725, 1998. 34096

Weiss, S. A., MacGorman, D. R., and Calhoun, K. M.: Lightning in the anvils of supercell thunderstorms, Mon. Weather Rev., 140, 2064–2079, 2012. 34093

Title Page

Abstract | Introduction

Conclusions | References

Tables | Figures

|◄ | ►|

◄ | ►

Back | Close

Full Screen / Esc

Printer-friendly Version

Interactive Discussion

Wennberg, P. O., Hanisco, T. F., Jaeglé, L., Jacob, D. J., Hintsa, E. J., Lanzendorf, E. J., Anderson, J. G., Gao, R.-S., Keim, E. R., Donnelly, S. G., Del Negro, L. A., Fahey, D. W., McKeen, S. A., Salawitch, R. J., Webster, C. R., May, R. D., Herman, R. L., Proffitt, M. H., Margitan, J. J., Atlas, E. L., Schauffer, S. M., Flocke, F., McElroy, C. T., and Bui, T. P.: Hydrogen radicals, nitrogen radicals and the production of O_3 in the upper troposphere, Science, 279, 49–53, doi:10.1126/science.279.5347.49, 1998. 34121

Wesely, M. L.: Parameterization of surface resistances to gaseous dry deposition in regional-scale numerical models, Atmos. Environ., 23, 1293–1304, 1989. 34096

WMO: Scientific Assessment of Ozone Depletion: 1998, Tech. rep., World Meteorological Organization, Geneva, Switzerland, 1999. 34093

Yevich, R. and Logan, J. A.: An assessment of biofuel use and burning of agricultural waste in the developing world, Global Biogeochem. Cy., 17, 1095, doi:10.1029/2002GB001952, 2003. 34096

Yienger, J. J. and Levy, H.: Empirical model of global soil-biogenic NO_x emissions, J. Geophys. Res., 100, 11447–11464, 1995. 34096

Zhang, Q., Streets, D. G., Carmichael, G. R., He, K. B., Huo, H., Kannari, A., Klimont, Z., Park, I. S., Reddy, S., Fu, J. S., Chen, D., Duan, L., Lei, Y., Wang, L. T., and Yao, Z. L.: Asian emissions in 2006 for the NASA INTEX-B mission, Atmos. Chem. Phys., 9, 5131–5153, doi:10.5194/acp-9-5131-2009, 2009. 34096

Zhang, R., Tie, X., and Bond, D. W.: Impacts of anthropogenic and natural NO_x sources over the U. S. on tropospheric chemistry, P. Natl. Acad. Sci. USA, 100, 1505–1509, 2003. 34093

Modeling lightning-NO$_x$ chemistry at sub-grid scale

A. Gressent et al.

Title Page

Abstract | Introduction

Conclusions | References

Tables | Figures

|◄ | ►|

◄ | ►

Back | Close

Full Screen / Esc

Printer-friendly Version

Interactive Discussion

Discussion Paper | Discussion Paper | Discussion Paper | Discussion Paper

A. Gressent et al.

Title Page

Abstract | Introduction

Conclusions | References

Tables | Figures

|◀ | ▶|

◀ | ▶

Back | Close

Full Screen / Esc

Printer-friendly Version

Interactive Discussion

Table 1. The initial atmospheric parameters and background concentrations of chemical species from GEOS-Chem outputs for the DSMACC chemical box model simulations.

	TEMP	PRESS	O_3	NO	NO_2	HNO_3	HNO_4	PAN	N_2O_5	CO
Units	(K)	(hPa)	(ppb)	(ppb)	(ppb)	(ppb)	(ppb)	(ppb)	(ppt)	(ppb)
Midlatitudes	228	313	67	0.04	0.01	0.15	0.02	0.1	2	94
Tropics	240	313	26	0.03	0.003	0.02	0.006	0.03	2.3	93

	OH	HO_2	H_2O_2	CH_2O	CH_4O_2	C_3H_8	C_5H_8	C_2H_4O	C_3H_6O
Units	(ppb)	(ppt)	(ppt)	(ppb)	(ppb)	(ppb)	(ppb)	(ppb)	(ppb)
Midlatitudes	0.2	4	0.4	0.06	0.1	0.47	0	7.5	4
Tropics	0.06	6	0.34	0.03	0.17	0.13	7.5	7.5	4

Printer-friendly Version

Interactive Discussion

Table 2. The plume lifetime τ (h) calculated for midlatitudes and tropics depending on the initial NO mixing ratio injected by lightning emissions (NO$_i$, ppb) and the horizontal diffusion coefficient (D_h, m^2 s^{-1}) for day (upper table) and night conditions (bottom table).

	Day					
τ (h)	Midlatitudes			Tropics		
NO$_i$ (ppb)	0.7	3.4	10	2.8	10	29.7
$D_h = 0.1$ (m^2 s^{-1})	1.55	8.14	23.9	4.40	23.1	67.9
$D_h = 15$ (m^2 s^{-1})	0.1	3.17	18.6	0.27	8.90	52.8
$D_h = 100$ (m^2 s^{-1})	0.01	0.47	4.17	0.04	1.32	11.7
	Night					
τ (h)	Midlatitudes			Tropics		
NO$_i$ (ppb)	0.7	3.4	10	2.8	10	29.7
$D_h = 0.1$ (m^2 s^{-1})	1.62	8.19	24.1	4.74	23.4	68.5
$D_h = 15$ (m^2 s^{-1})	0.31	6.19	22	2.77	21.3	66.4
$D_h = 100$ (m^2 s^{-1})	0.05	1.23	10.6	0.43	10.5	55.4

Table 3. The effective reaction rate constant K_{eff} (10^{-19} molecules^{-1} s^{-1} cm^{-3}) in midlatitudes and tropics depending on the initial NO mixing ratio injected by lightning emissions (NO$_i$, ppb) and the horizontal diffusion coefficient (D_h, m^2 s^{-1}) for day (upper table) and night conditions (bottom table).

Day						
K_{eff} (10^{-19} molecules^{-1} s^{-1} cm^{-3})	Midlatitudes			Tropics		
NO$_i$ (ppb)	0.7	3.4	10	2.8	10	29.7
$D_h = 0.1$ (m^2 s^{-1})	1.28	1.24	1.51	0.77	1.2	1.83
$D_h = 15$ (m^2 s^{-1})	8.44	5.49	5.43	7.79	3.64	4.13
$D_h = 100$ (m^2 s^{-1})	12.1	16.4	14.4	23	19.8	13
Night						
K_{eff} (10^{-19} molecules^{-1} s^{-1} cm^{-3})	Midlatitudes			Tropics		
NO$_i$ (ppb)	0.7	3.4	10	2.8	10	29.7
$D_h = 0.1$ (m^2 s^{-1})	1.28	1.24	1.51	0.77	1.10	1.83
$D_h = 15$ (m^2 s^{-1})	4.84	4.55	5.43	2.3	2.98	4.13
$D_h = 100$ (m^2 s^{-1})	7.36	8.39	6.73	6.45	3.94	5.16

Table 4. The fractions of NO_x conversion into HNO_3 within the plume (β_1 and β_2) in midlatitudes and tropics depending on the initial NO mixing ratio injected by lightning emissions (NO_i, ppb) and on particles for day (upper table) and night conditions (bottom table).

	Day					
β_1 (10^{-4})	Midlatitudes			Tropics		
NO_i (ppb)	0.7	3.4	10	2.8	10	29.7
Aerosols	2.53	3.34	3.45	2.51	2.95	2.6
Ice	0.23	0.3	0.3	0.2	0.23	0.3
Mean	1.38	1.8	1.88	1.34	1.59	1.47
	Night					
β_2 (10^{-3})	Midlatitudes			Tropics		
NO_i (ppb)	0.7	3.4	10	2.8	10	29.7
Aerosols	14.3	9.89	8	4.9	1.69	0.24
Ice	14.4	9.96	8.06	4.89	1.70	0.24
Mean	14.4	9.92	8.03	4.88	1.7	0.24

Table 5. Values of the parameters for the plume parameterization corresponding to the experiments P1 and P2.

Parameters					Experiments							
					P1					P2		
D_h (m^2 s^{-1})		0.1			15			100			15	
NO$_i$ (ppb)	Min	Mean	Max	Min	Mean	Max	Min	Mean	Max		Mean	
Midlatitudes	0.7	3.4	10	0.7	3.4	10	0.7	3.4	10		3.4	
Tropics	2.8	10.2	29.7	2.8	10.2	29.7	2.8	10.2	29.7		10.2	
β_1					Mean					0	Min	Mean	Max
β_2					Mean					0	Min	Mean	Max

Table 6. The variability of NO$_x$ (in ppt) and O$_3$ (in ppb) depending on the horizontal diffusion coefficient (D_h, m^2 s^{-1}) and on the NO$_i$ mixing ratio (ppb) injected by lightning for midlatitudes (Florida and North Atlantic) and tropics (Congo and South Atlantic) in January and July.

| | January | | | | July | | | |
| | Midlatitudes | | Tropics | | Midlatitudes | | Tropics | |
	Florida	North Atlantic	Congo	South Atlantic	Florida	North Atlantic	Congo	South Atlantic
ΔNO$_x$±	[−1.7; +1.8]	[−8.2; +1.7]	[−33.1; +29.7]	[−6.5; +6.9]	[−9.3; +5.4]	[−21.1; +6.6]	[−14.3; +21]	[−11.5; +2.6]
ΔO$_3$±	[−0.16; +0.72]	[−0.12; +0.53]	[−1.56; +2.16]	[−0.49; +0.94]	[−0.44; +1.01]	[−0.49; +0.66]	[−1.18; +1.93]	[−0.14; +0.92]

Table 7. The variability of NO$_x$ (in ppt, $\times 10^{-2}$) and O$_3$ (in ppb, $\times 10^{-4}$) depending on β_1 and β_2 values for midlatitudes (Florida and North Atlantic) and tropics (Congo and South Atlantic) in January and July. Experiment P1, using $D_\mathrm{h} = 15\,\mathrm{m}^2\,\mathrm{s}^{-1}$ and NO$_i^\mathrm{mean}$, performed with the GEOS-Chem model.

	January				July			
	Midlatitudes		Tropics		Midlatitudes		Tropics	
	Florida	North Atlantic	Congo	South Atlantic	Florida	North Atlantic	Congo	South Atlantic
ΔNO$_x$±	[−1.6; −0.06]	[−2.3; −2.3]	[−2.3; +0.9]	[+0.3; +0.6]	[−3.3; +1.4]	[−21.1; +6.6]	[+0.4; +2.1]	[−0.9; −0.4]
ΔO$_3$±	[−9; +5]	[−9; +4]	[−3; +22]	[−10; +11]	[−24; −6]	[−6; +19]	[−8; +17]	[−30; −2]
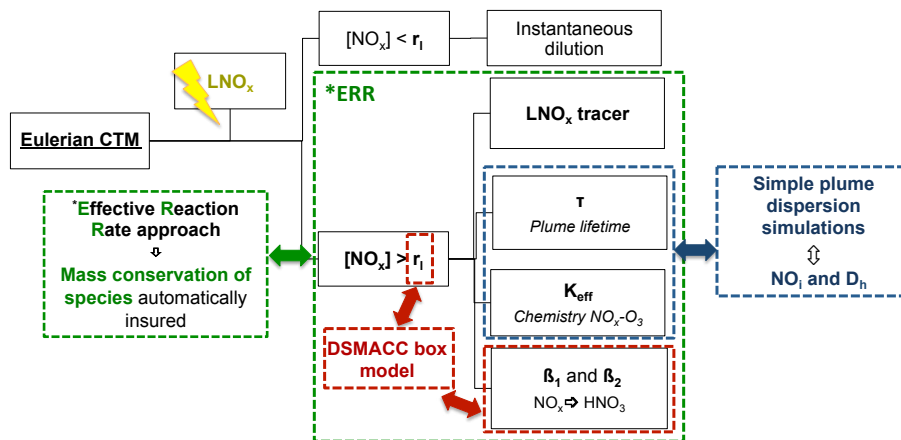
Figure 1. The lightning NO$_x$ plume parameterization based on the Effective Reaction Rate approach.
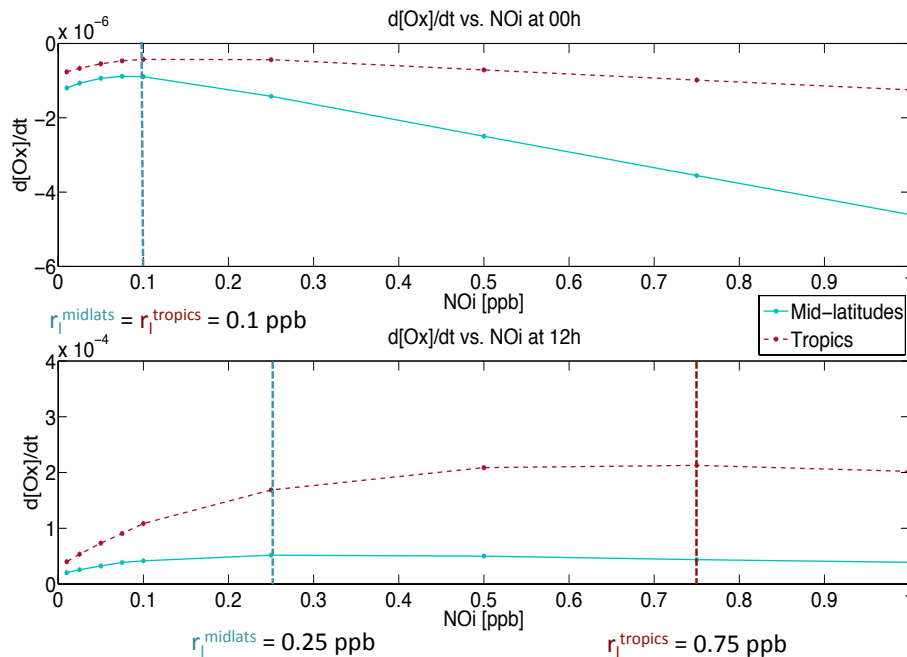
Figure 2. r_l critical value and odd oxygen trends from DSMACC chemistry box model simulations for midlatitudes (solid line) and tropics (dotted line) **(a)** at midnight (upper panel) and **(b)** at midday (bottom panel).
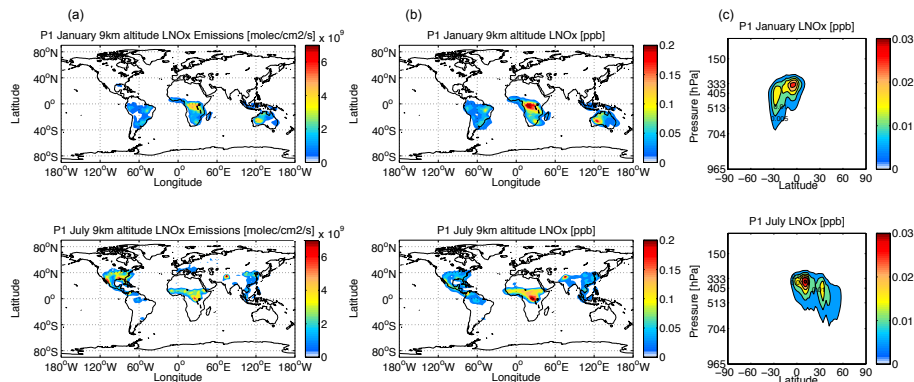
Figure 3. (left panels, **a**) Geographical distributions at 9 km altitude of lightning NO$_x$ emissions, (middle panels, **b**) the geographical distributions of the related LNO$_x$ tracer (in ppb) and (right panels, **c**) the zonal averaged of the LNO$_x$ tracer (in ppb), for January (top) and July (bottom). Experiment P1, using $D_{\mathrm{h}} = 15\,\mathrm{m^2\,s^{-1}}$ and NO$_i^{\mathrm{mean}}$, performed with the GEOS-Chem model.
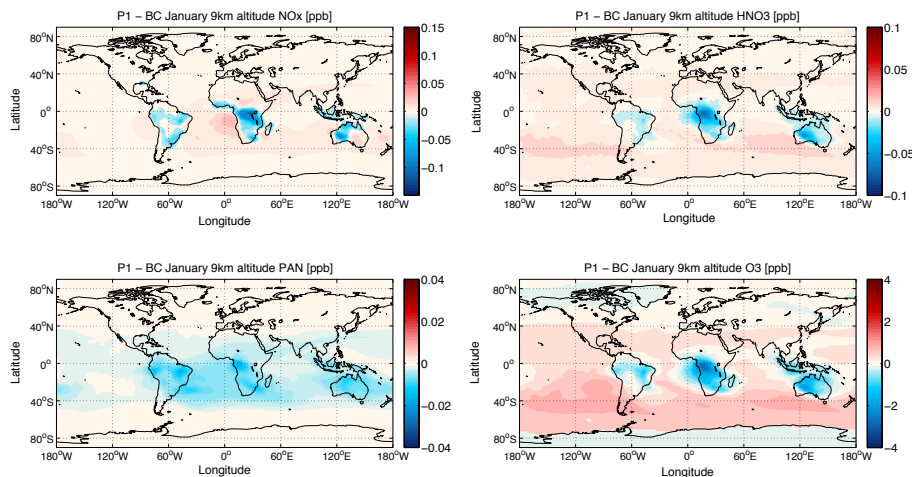
Figure 4. Geographical distributions of NO$_x$, HNO$_3$, PAN, and O$_3$ variations (in ppb) at 9 km altitude for January from the absolute difference between P1 and BC experiments. P1 was performed using $D_h = 15\,\text{m}^2\,\text{s}^{-1}$ and NO$_i^{\text{mean}}$ with GEOS-Chem.
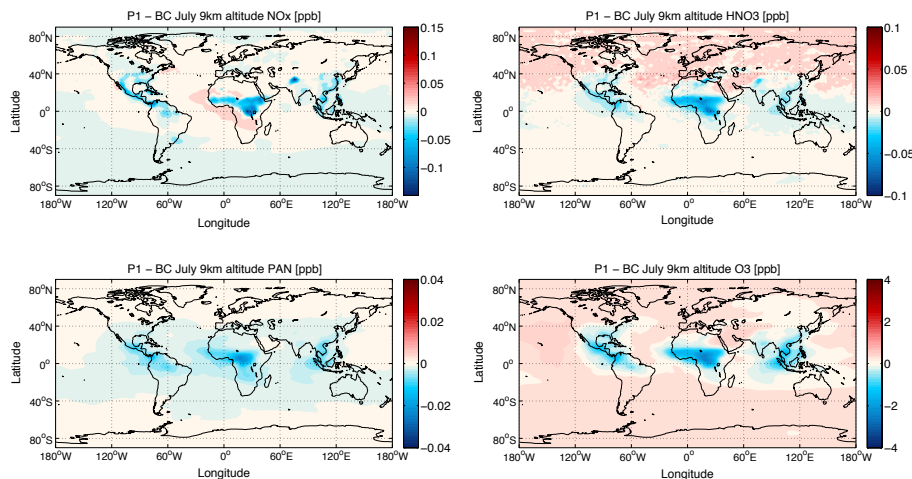
Figure 5. Geographical distributions of NO$_x$, HNO$_3$, PAN, and O$_3$ variations (in ppb) at 9 km altitude for July from the absolute difference between P1 and BC experiments. P1 was performed using $D_h = 15\,\text{m}^2\,\text{s}^{-1}$ and NO$_i^{\text{mean}}$ with GEOS-Chem.
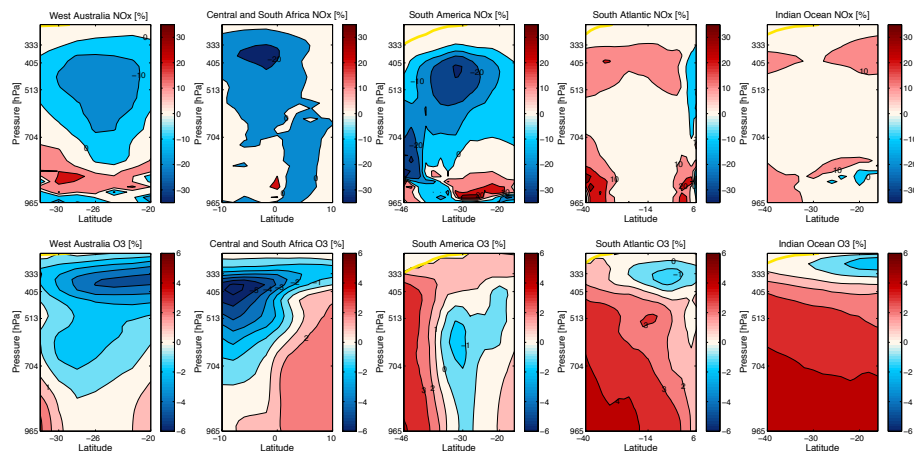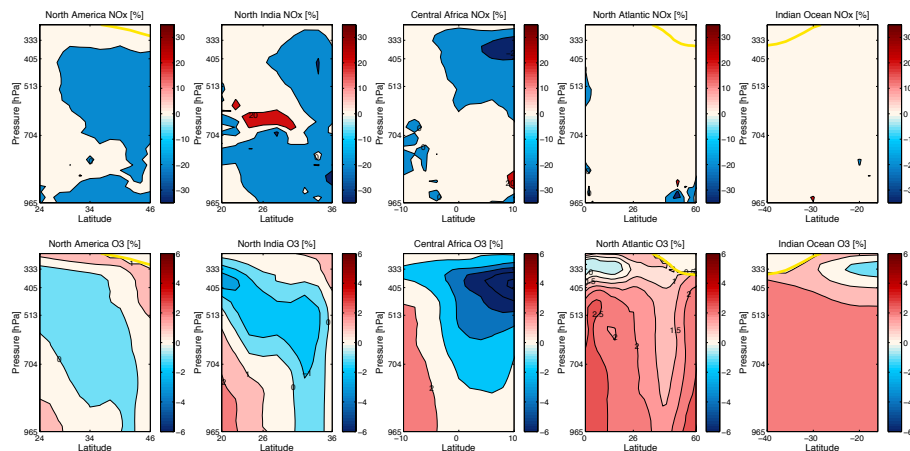
Figure 6. Zonal averaged NO$_x$ (upper panels) and O$_3$ (bottom panels) variations (in %) over the regions characterized by strong NO$_x$ emissions for January (the yellow solid line represents the tropopause level), from the relative difference between P1 and BC experiments ((P1–BC) /BC). P1 was performed using D_h = 15 m^2 s^{-1} and NO$_i^{\text{mean}}$ with GEOS-Chem.

Figure 7. Zonal averaged NO$_x$ (upper panels) and O$_3$ (bottom panels) variations (in %) over the regions characterized by strong NO$_x$ emissions for July (the yellow solid line represents the tropopause level), from the relative difference between P1 and BC experiments ((P1–BC) /BC). P1 was performed using $D_h = 15\,\mathrm{m}^2\,\mathrm{s}^{-1}$ and NO$_i^{mean}$ with GEOS-Chem.

Full Screen / Esc

Printer-friendly Version

Interactive Discussion
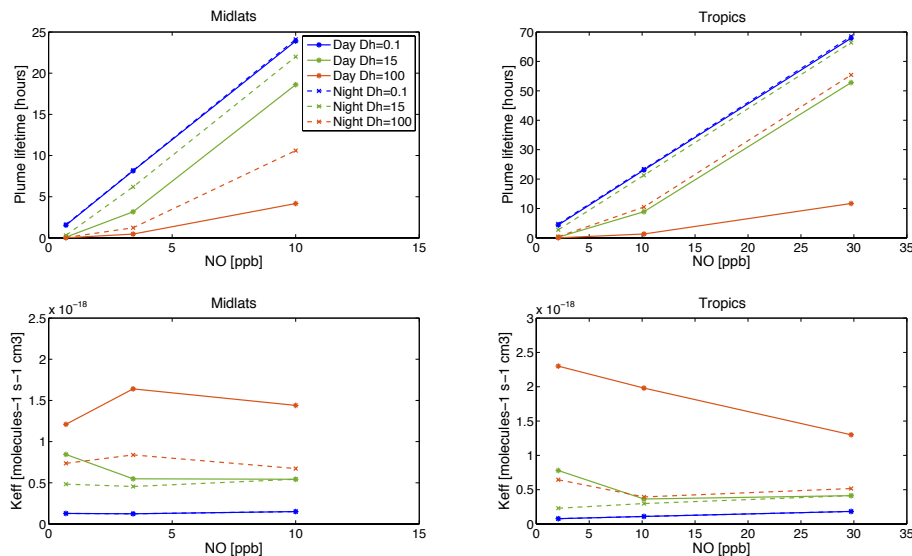
Figure 8. The plume lifetime (τ, upper panels) and the effective reaction rate constant (K_{eff}, bottom panels) depending (i) on the horizontal coefficient diffusion (D_{h}, m^2 s^{-1}) for midlatitudes (left panels) and tropics (right panels) and (ii) on the NO mixing ratio injected by lightning (NO$_i$, in ppb).
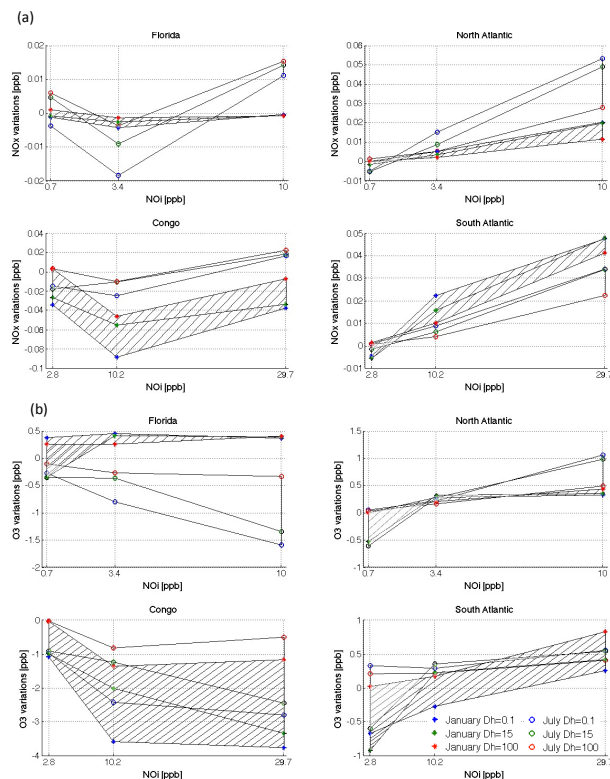
Figure 9. The NO$_x$ **(a)** and O$_3$ **(b)** variability at 9 km altitude depending on the horizontal co-efficient diffusion (D_h, m^2 s^{-1}) and on the NO mixing ratio injected by lightning (NO$_i$, ppb) for midlatitudes (Florida and North Atlantic) and tropics (Congo and South Atlantic). Intervals are hatched in January and non-hatched in July. Markers correspond to the NO$_x$ variations simulated for D_h = 0.1 m^2 s^{-1} (red ones), D_h = 15 m^2 s^{-1} (blue ones) and D_h = 100 m^2 s^{-1} (green ones).